Materials aspects of hydro-abrasive wear in the dredging industry

Liu, Yueting

DOI
10.4233/uuid:71da5266-8d7a-4143-91de-d2284fb02639

Publication date
2017

Document Version
Final published version

Citation (APA)
Liu, Y. (2017). *Materials aspects of hydro-abrasive wear in the dredging industry*. [Dissertation (TU Delft), Delft University of Technology]. https://doi.org/10.4233/uuid:71da5266-8d7a-4143-91de-d2284fb02639

MATERIALS ASPECTS OF HYDRO-ABRASIVE WEAR IN THE DREDGING INDUSTRY

Yueting LIU

MATERIALS ASPECTS OF HYDRO-ABRASIVE WEAR IN THE DREDGING INDUSTRY

Proefschrift

ter verkrijging van de graad van doctor

aan de Technische Universiteit Delft,

op gezag van de Rector Magnificus K.C.A.M. Luyben,

voorzitter van het College voor Promoties,

in het openbaar te verdedigen op

Maandag 25 September 2017 om 15:00 uur

door

Yueting LIU

Master of Science in Materials Science and Engineering
University of Science and Technology Beijing, Beijing, China,
geboren te Pingdingshan, China.

This dissertation has been approved by the

promotor: prof. dr. G.C.A.M. Janssen

Composition of the doctoral committee:

Rector Magnificus,	Chairman
Prof. dr. G.C.A.M. Janssen,	Technische Universiteit Delft, promotor
Independent members:	
Prof. dr. S. van der Zwaag	Technische Universiteit Delft
Prof. dr. H. Terryn	Vrije Universiteit Brussel
Prof. dr. G. Palasantzas	University of Groningen
Prof. dr. J. Sietsma	Technische Universiteit Delft
Prof. dr. C. van Rhee	Technische Universiteit Delft
Dr. J.M.C. Mol	Technische Universiteit Delft

This research was carried out under project number M33.3.11427b in the framework of the Research Program of the Materials innovation institute (m2i) in the Netherlands (www.m2i.nl)

Keywords: Wear, corrosion, surface roughness, micro coupling, carbon enrichment, cathodic protection

Printed by: Gildeprint, The Netherlands

ISBN 978-94-91909-46-7

An electronic version of this dissertation is available at
http://repository.tudelft.nl/.

To my parents and my sister

致我的父母和姐姐

Contents

1

Introduction

I never allow myself to have an opinion on anything of which I do not know the arguments on the other side better than they do

Charlie Munger

1

1.1. Background

Dredging technology has resulted in many significant contributions to the infrastructure of the world. Some notable achievements include canals, like the Suez and Panama Canals, and islands like the amazing palm island. One of the important parts of dredging is slurry transport. In slurry transport, pipelines are used to transport the mixture of sand or other solids and liquids. During the transport process, corrosive and abrasive wear occur, and often these joint processes lead to severe damage to the pipelines.

1.2. Dreding and slurry transport

Dredging is an activity, usually performed underwater in freshwater areas or seas, to re-locate the bottom sediments to a different place. Dredging engineering benefits the infrastructure of the world [1–5]. First, dredging is used to keep waterways navigable. Moreover, dredging is used to replenish materials for construction work. Finally, dredging is used as a powerful tool for land reclamation. In the past decades, dredging engineering has led to successful land reclamation in many countries, e.g., the Netherlands, China, United Arabic Emirates.

In dredging engineering, slurry transport is a critical process and has been studied for decades due to its complexity and significance [6, 7]. Slurry is essentially a mixture of a carrying fluid and solid particles held in suspension. The physical characteristics of slurry are dependent on many factors such as size and distribution of particles, the concentration of solids, the level of turbulence, temperature and viscosity of the liquid. In addition to the complex physical characteristics, the composition of slurries is diverse (i.e., multiple combinations of different solids and liquids). The size of the solid in a slurry varies (typically from tens of microns to centimeters). Empirical and mathematical models are required to describe the transportation process. Experimental work is necessary to validate the models and guide the design

of pipelines.

In slurry transport, there are two common types of flow: homogeneous and heterogeneous flow. As shown in Figure 1.1, for homogeneous flow, solids are uniformly distributed throughout the liquid carrier. The particles are very fine, and the typical size is smaller than 40 μm. The concentration of the particles is high (typically 50%-60% by weight). As the concentration of particles increases (beyond 40% by weight for many slurries), the mixture becomes more viscous. Due to the high viscosity of the slurry and the small size of the particles, the required velocity to keep the slurry homogenous is low. Drilling mud, sewage sludge, and fine limestone behave as homogeneous flows. By comparison, in a heterogeneous flow, solids are not uniformly mixed, and the concentration increases along the perpendicular direction from top to bottom. Dunes or a sliding bed may form in the pipe, with the distribution that heavier particles sink to the bottom and the lighter ones remain suspended in the liquid. Heterogeneous slurries typically exist in placer mining (the mining of stream bed deposits for minerals), phosphate rock mining, dredging applications, and tailing disposal (the disposal of the materials left over after separating the useful fraction from ore). Given the large particle size and the strong tendency of settling, the concentration in heterogeneous flow is low, and the speed is high to keep the flow from forming a stationary bed. Specifically, the typical concentration is below 25% by weight in dredging applications and below 35% by weight in tailing disposal applications; Heterogeneous flows require a minimum carrier velocity termed deposition velocity, below which, a stationary bed forms. In some tailing applications of the Taconite mines of Minnesota, the typical deposition velocity is 3.4-4m/s [8, 9].

One of the main problems during slurry transport is that the joint process of corrosion and wear leads to a drastically short lifetime of slurry pipelines.

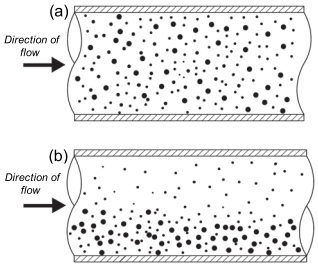

Figure 1.1: (a) Homogeneous flow, the solids are uniformly mixed in the flow and uniformly distributed along the vertical direction; (b)Heterogeneous flow, the solids are not uniformly mixed. The large particles sink to the bottom, and the small ones suspend in the flow. The distribution of the particles, along the vertical direction, is not uniform either. The particle concentration increases from top to bottom. A sliding bed might form, but no stationary bed forms once the velocity is above the deposition velocity (a required velocity for heterogeneous flow to prevent the formation of stationary bed)

1.3. Corrosion and wear during slurry transport

Corrosion and wear of slurry pipelines are two key problems in slurry transport, and often these two processes occur simultaneously. The simultaneous occurrence of corrosion and wear is classified as tribocorrosioin: the study of the influence and interaction of mechanical, chemical/electrochemical or biological environmental factors on the friction and wear performance of materials [10]. The material damage caused by tribocorrosion is not merely the summation of the damage due to wear factors and the damage due to corrosion factors, as the interaction between corrosion and wear plays an important role in the complex tribocorrosion system [11]. As shown in Figure 1.2 the tribocorrosion system contains many components, e.g., mechanical conditions (load, velocity), materials properties (Hardness, roughness). Wear is reported to be able to modify the sensitivity of the materials to corrosion. Also, corrosion can affect the wear resistance of materials by altering the surface contact condition [12]. The interaction is reported to usually expedite the degradation of the material [13–18].

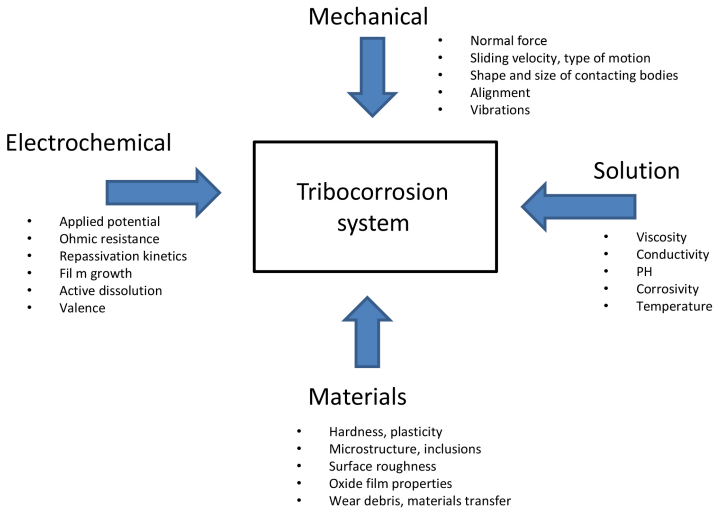

Figure 1.2: tribocorrosion system and relevant parameters [19]

W. Batchelor and G. W. Stachowiak in 1988 measured the wear rates of mild steel, zinc, and magnesium under simultaneous abrasion and corrosion [15]. They found out that the interaction between corrosion and abrasive wear occurs when the static corrosion rate is more than half the time-based abrasion rate (i.e., the abrasive wear rate quantified by volume loss per unit time instead of per unit distance). At the same time, similar work was done by B. W. Madsen [20]. Madsen used a slurry wear test apparatus, developed by the Bureau of Mines, to measure the abrasion-corrosion interaction. The silica sand and aqueous solution were continuously fed into the test chamber, and subsequently, the specimens, inside the chamber, were abraded and corroded simultaneously. The specimens were low alloy steel, stainless steel, and wear-resistant low alloy steel. Madsen conducted three types of tests to measure the total abrasive-corrosive wear rate, the wear rate due to abrasive wear only, and the electrochemical corrosion rate. The total wear rate was determined by weight loss method. The wear rate due to abrasion was obtained while the specimen was cathodically protected (which creates

a pure abrasive wear environment without corrosion). The electrochemical corrosion rate was determined by using polarization scans during slurry wear tests. The results of this work showed a strong interaction between abrasive wear and corrosion, as the total wear rate was much larger than the summation of the two individual components.

B.T Lu and J.L. Luo studied the plastic deformation and anodic dissolution of a carbon steel subjected to tribocorrosion [21]. They found that plastic deformation can alter the anodic dissolution rate of the sample. Conversely, the anodic current can reduce the wear resistance of the material surface layer, as observed by the degradation of hardness after experiments. The hardness degradation, in this study, was found proportional to the logarithm of anodic current density. This work provides a quantitative relationship between mechanical (plastic deformation) and electrochemical components (anodic dissolution).

A galvanic micro cell can form between the worn area and the unworn area during tribocorrosion and subsequently a current exists in the micro cell within the sample. The reason lies in the potential difference between the depassivated worn area and the passivated unworn area of the sample. The corrosion rate of the sample is typically calculated from the current by using Faraday's law of electrolysis. Therefore, the current of the micro cell within the sample can lead to a wrong measurement of the current of the sample in the tribocorrosion system, and consequently, the formation of a micro cell can result in a wrong calculation of the corrosion rate. Several researchers have reported this problem [22–24]. In 1995, A. Sakamoto, H. Funaki, and M. Matsumura tested several materials under cavitation erosion [23]. Their main conclusion is that the corrosion rate increases when a galvanic cell forms between the cavitation damaged area (anode) and undamaged area (cathode). Therefore the corrosion rate calculated from anodic density is not necessarily equal to the real value. Landolt and his co-workers, in a study in 2001, connected two originally identical samples, through a zero

resistance ammeter(ZRA), to monitor the galvanic current during corrosive, abrasive wear [22]. After starting the wear process, a current was observed between the two originally identical samples. This work evidences the fact that a galvanic cell exists between worn and unworn areas of the sample when subject to tribocorrosion.

Passivity (the formation of a non-conductive surface film) of materials accelerates the wear rate in tribocorrosion system. S. Mischler and co-workers studied the role of passive oxide films on the wear of steel in tribocorrosion systems [25]. The sample was electrochemically polarized while rubbing against a counter body. During the experiments, the surface chemistry (more specifically, the formation of surface oxide film) was well controlled to determine the relative contribution of mechanical(wear) and chemical(corrosion) factors on the overall degradation. They found that the formation of a passive film increased the overall wear rate. The formation of the passive film, which typically protects the material from corrosion, accelerates the wear rate in tribocorrosion system.

Passivity is determined by the alloying elements in the material. Elements that have a high metal-oxygen bond strength and low metal-metal bond strength promote passivation. The high metal-oxygen bond strength is responsible for the stability of the passive film. The low metal-metal bond strength makes the bond easy to break, and the breaking favors the rapid nucleation and growth of the oxide film, especially during early stages of passivation. In contrast, elements that possess a high metal-metal bond strength and a low metal-oxygen strength inhibit passivation [26].

1.4. Common techniques and standards

Over the years, various techniques have been widely used to study the combined effect of corrosion and wear. The techniques are classified into two main categories: in-situ techniques and ex-situ techniques. In-situ tech-

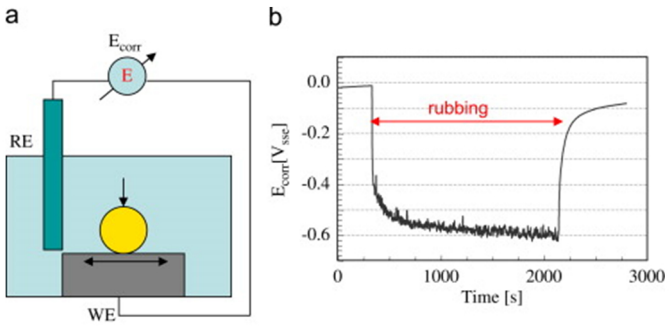

Figure 1.3: (a) Schematic view of an OCP technique(reference electrode, standard silver chloride electrode, SSE); (b) Evolution of the corrosion potential of a Ti6Al4V alloy rubbing against an alumina ball in 0.9% NaCl solution [27]

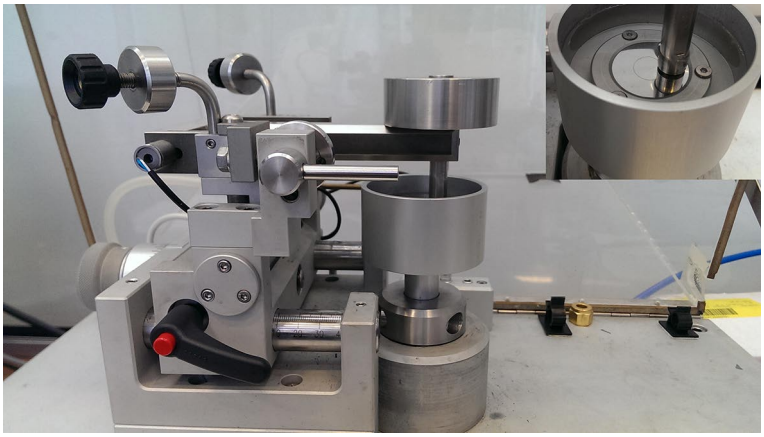

Figure 1.4: Pin on disc tribometer

niques provide instant measurement or control, including open circuit potential measurements (OCP), polarization curves, impedance spectroscopy, and noise measurements. The ex-situ techniques provide characterization of the samples before or after experiments, including optical microscopy (OM), scanning electron microscopy (SEM), microhardness measurements, and chemical analysis. In-situ techniques to study corrosion are mainly electrochemical techniques. Electrochemical techniques are increasingly applied in tribocorrosion experiments, and they provide unique advantages, e.g., the convenient observation of how wear affects corrosion kinetics (by observing the current evolution) [17, 19, 27, 28]. Figure 1.3 shows the typical open circuit potential measurement. In 2001, Tribology Committee of the CEFRACOR (Centre Français de l'Anti-Corrosion, Paris) organized an inter-laboratory investigation on tribo-electrochemical measurements [29]. Seven European laboratories participated in this investigation, aiming to evaluate the reproducibility and comparability of electrochemical techniques. Several tests were carried out including polarization curves, polarization curves during rubbing, friction test, friction test at an applied electrochemical potential. Results showed that the reproducibility at laboratory level was good for both tribological and electrochemical parameters. This study rationalizes and promotes the use of in-situ electrochemical techniques.

Pin on disc tribometer is used to perform abrasive corrosive experiments. A tribometer is an instrument that measures friction coefficient, friction force, and wear depth. It was first invented by Dutch scientist Musschenbroek in the 18th century [30]. A pin on disc tribometer, shown in Figure 1.4, consists of a stationary pin (or a ball holder to hold a ball) under a certain load and a rotary disc (subfigure at the top right). The coefficient of friction is calculated by dividing the friction force (tangential force) by the loading force. A liquid holder can provide a corrosive environment.

Ex-situ techniques are also widely used in studying tribocorrosion. Techniques like microhardness measurement, optical and scanning electron mi-

croscopy have proved useful. For instance, hardness measurement is a convenient technique to measure the work hardening of the sample after tribocorrosion. Other techniques like XPS and EDS can be used to analyze the composition of the corrosion products. Additionally, some well-documented standards provide guidance for designing and performing tribocorrosion experiments, as listed in Table 1.1.

Table 1.1: Standards related to tribocorrosion

Standard	Description
ASTM G 99-95a	Standard test method for wear testing with a pin on disk apparatus
ASTM G 133-95	Standard test method for linear reciprocating ball on flat sliding wear
ASTM G 77-93	Standard test method for ranking resistance of materials to sliding wear using block-on-ring wear test
ISO 20808	Fine ceramic(advanced ceramics, advanced technical ceramics)- determination of friction and wear characteristics of monolithic ceramics by ball-on-disk method
DIN 50324	Tribology; testing of friction and wear model test for sliding friction of solids(ball-on-disk system)
DIN 51834-1	Testing of lubricants- Tribological test in the translator oscillation apparatus
ASTM G 119-04	Standard guide for determining synergism between wear and corrosion

1.5. Scope and outline of the thesis

Wear and corrosion are two old and costly problems. When coupled together, the degradation becomes a more complex issue that requires a deep understanding of the interaction between the two processes. The project originates from dredging industry, where slurries, generated during dredging process, need to be transported through pipelines. The pipelines wear dramatically during slurry transport. To tackle the problem, knowledge from three perspectives is essential: the slurry properties, the flow regime, and materials response. The aim of this PhD thesis is to gain a better understanding of the wear mechanism from materials perspective.

The thesis consists of six chapters. The first chapter provides a general introduction to this research, including the background of dredging and slurry transport, the identification of the problem due to the joint corrosion and wear processes, and the common techniques used to study the mechanisms.

Chapter 2 presents the mechanism of cyclic formation and removal of corrosion films. This chapter starts with an introduction to the wear problem and details of the experimental setup. The material used in this chapter is aluminum alloy 7075T6, which has a specific strength comparable with high strength steel. The experiments consist of two series: one series uses various liquids with a difference in corrosivity, and the other series uses various imposed electrochemical potentials to vary corrosivity. The wear mechanism, in this study, is concluded to be the cyclic formation and removal of surface corrosion film, which leads to higher wear rate while corrosion is present.

Chapter 3 presents the wear study in slurry loop. The experiments were performed in both fresh water and sea water with two different particles. The wear of the samples is represented by the surface roughness. The surface roughness of the sample can be fully attributed to wear since, before each experiment, the sample was polished until mirror-like (roughness

close to zero). In this study, no noticeable difference in wear was found between the samples subjected to fresh water and sea water, although they have different corrosivity. Additionally, the sample mounting turned out to be of great importance because if the mounting is not flush with the wall, the samples wear non-uniformly as observed with the large particle set of experiment.

Chapter 4 presents the wear mechanism of galvanic mico-coupling. This mechanism was never reported before this study, and it is distinctively different from the mechanism of cyclic formation and removal of surface films. The material is a structural steel with a yield strength of 235 MPa (S235). The microstructure of S235 contains two phases: ferrite and pearlite. Pearlite contains ferrite and cementite. When the two phases are immersed in a corrosive environment, they form micro couples due to their electrochemical potential difference. The micro coupling leads to the dissolution of ferrite and consequently the protruding of cementite. The cementite is redistributed due to wear. Since cementite is much harder than ferrite, the modified sample surface is more wear resistant than the original surface. The main conclusion is that the interaction between corrosion and wear can be beneficial once micro-coupling forms and leads to the harder phase to be redistributed on the material surface.

Chapter 5 presents the influence of impacting on the wear mechanism of the same steel used in chapter 4. Impacting plays a major role in wear, where abrasion and corrosion co-exist. A hammering module is employed to provide impacting effect, and the effect is quantified by the lifted height of the hammer. The conclusion of this study is that when the impacting effect is small, the wear mechanism of micro-coupling (presented in chapter 4) still holds and the sample wears the least in sea water. However when the impacting effect is large, the influence of corrosion will be less significant, and the wear rates in various liquids are comparable.

Chapter 6 presents the general conclusions and provides directions for future

work. Finally, the results of the complete research are summarized in chapter summary.

References

[1] K. M. Cooper, C. R. S. Barrio Froján, E. Defew, M. Curtis, A. Fleddum, L. Brooks, and D. M. Paterson, *Assessment of ecosystem function following marine aggregate dredging,* Journal of Experimental Marine Biology and Ecology **366**, 82 (2008).

[2] D. D. Dickerson, D. A. Nelson, G. Banks, and R. M. Engler, *Environmental Effects of Dredging,* Technical Note EEDP-09-6 , 14 (1990).

[3] P. L. A. Erftemeijer and R. R. Robin Lewis, *Environmental impacts of dredging on seagrasses: A review,* Marine Pollution Bulletin **52**, 1553 (2006).

[4] J. C. Kromkamp and J. Peene, *Changes in phytoplankton biomass and primary production between 1991 and 2001 in the Westerschelde estuary (Belgium/The Netherlands),* Hydrobiologia **540**, 117 (2005).

[5] X. Y. Wang and J. Feng, *Assessment of the effectiveness of environmental dredging in South Lake, China,* Environmental Management **40**, 314 (2007).

[6] M. Kadja and G. Bergeles, *Modelling of slurry droplet drying,* Applied Thermal Engineering **23**, 829 (2003).

[7] J. M. LeBeau and Y. Boonyongmaneerat, *Comparison study of aqueous binder systems for slurry-based processing,* Materials Science and Engineering A **458**, 17 (2007).

[8] P. Doron and D. Barnea, *A three-layer model for solid-liquid flow in horizontal pipes,* International Journal of Multiphase Flow **19**, 1029 (1993).

[9] P. Doron, D. Granica, and D. Barnea, *Slurry flow in horizontal pipes-experimental and modeling,* International Journal of Multiphase Flow **13**, 535 (1987).

[10] J. Celis and P. Ponthiaux, *Introduction in" Testing tribocorrosion of passivating materials supporting research and industrial innovation: Handbook",* in *European Federation of Corrosion Series* (Maney Publishing, 2012).

[11] J. Jiang and M. M. Stack, *Modelling sliding wear: From dry to wet environments,* Wear **261**, 954 (2006).

[12] L. Benea, P. Ponthiaux, F. Wenger, J. Galland, D. Hertz, and J. Y. Malo, *Tribocorrosion of stellite 6 in sulphuric acid medium: Electrochemical behaviour and wear,* Wear **256**, 948 (2004).

[13] C. Allen, A. Ball, and B. Protheroe, *The abrasive-corrosive wear of stainless steels,* Wear **74**, 287 (1981).

[14] I. Iwasaki, S. Riemer, J. Orlich, and K. Natarajan, *Corrosive and abrasive wear in ore grinding,* Wear **103**, 253 (1985).

[15] A. Batchelor and G. Stachowiak, *Predicting synergism between corrosion and abrasive wear,* Wear **123**, 281 (1988).

[16] B. Matthes, E. Broszeit, and K. Kloos, *Tribological behaviour and corrosion performance of Ti-B-N hard coatings under plastic manufacturing conditions,* Surface and Coatings Technology **57**, 97 (1993).

[17] S. Watson, F. Friedersdorf, B. Madsen, and S. Cramer, *Methods of measuring wear-corrosion synergism,* Wear **181-183**, 476 (1995).

[18] M. Stemps, S. Mischler, and D. Landolt, *The effect of contact configuration on the tribocorrosion of stainless steel in reciprocating sliding under potentiostatic control,* Corrosion Science **45**, 625 (2003).

[19] D. Landolt, S. Mischler, and M. Stemp, *Electrochemical methods in tribocorrosion: A critical appraisal,* Electrochimica Acta **46**, 3913 (2001).

[20] B. W. Madsen, *Measurement of erosion-corrosion synergism with a slurry wear test apparatus,* Wear **123**, 127 (1988).

[21] B. T. Lu and J. L. Luo, *Synergism of electrochemical and mechanical factors in erosion-corrosion.* The journal of physical chemistry. B **110**, 4217 (2006).

[22] F. Galliano, E. Galvanetto, S. Mischler, and D. Landolt, *Tribocorrosion behavior of plasma nitrided Ti-6Al-4V alloy in neutral NaCl solution,* Surface and Coatings Technology **145**, 121 (2001).

[23] A. Sakamoto, H. Funaki, and M. Matsumura, *Influence of galvanic macro-cell corrosion on the cavitation erosion durability assessment of metallic materials-International cavitation erosion test of Gdansk,* Wear **186-187**, 542 (1995).

[24] S. S. Rajahram, T. J. Harvey, J. C. Walker, S. C. Wang, R. J. K. Wood, and G. Lalev, *A study on the evolution of surface and subsurface wear of UNS S31603 during erosion-corrosion,* Wear **271**, 1302 (2011).

[25] S. Mischler, a. Spiegel, and D. Landolt, *The role of passive oxide films on the degradation of steel in tribocorrosion systems,* Wear **225-229**, 1078 (1999).

[26] P. Marcus, *Surface science approach of corrosion phenomena,* Electrochimica Acta **43**, 109 (1998).

[27] S. Mischler, *Triboelectrochemical techniques and interpretation methods in tribocorrosion: A comparative evaluation,* Tribology International **41**, 573 (2008).

[28] P. Ponthiaux, F. Wenger, D. Drees, and J. P. Celis, *Electrochemical techniques for studying tribocorrosion processes,* Wear **256**, 459 (2004).

[29] S. Mischler and P. Ponthiaux, *A round robin on combined electrochemical and friction tests on alumina/stainless steel contacts in sulphuric acid,* Wear **248**, 211 (2001).

[30] Andersen Hemming, *Historic Scientific Instruments in Denmark* (The Royal Danish Academy Of Science And Letters, 1995).

2

Combined corrosion and wear of aluminum alloy 7075-T6

It does not matter how beautiful your theory is,
it does not matter how smart you are.
If it does not agree with experiment, it is wrong

Richard Feynman

This chapter is based on the following article:
Liu, Yueting, J. M. C. Mol, and G. C. A. M. Janssen. "Combined Corrosion and Wear of Aluminium Alloy 7075-T6." Journal of Bio-and Tribo-Corrosion 2, 9 (2016)

2

In this chapter, the wear mechanism of cyclic formation and removal of the surface corrosion products is presented. The combined effect of corrosion and wear, on the aluminum alloy 7075-T6, was studied. Two series of wear experiments were performed with various conditions and severity of corrosion environments: chemically by using ethanol, deionized water, and sea water, and electrochemically by applying various potentials using a potentiostat in sea water. Results show that, in sea water, the wear rate was higher than in deionized water and ethanol. In the potentiostat experiments, at the anodic potentials, the wear rates were higher than at the open circuit potential and the cathodic potentials. Sea water is the most corrosive one among the three liquids and the corrosion products can be easily removed. When applying anodic potentials, corrosion is accelerated, and the higher wear rate confirms that higher corrosion rate leads to higher wear rate due to the formation and removal of corrosion products during tribo-corrosion.

2.1. Introduction

The aluminum alloy 7075-T6 (AA7075-T6) is used extensively in engineering [1–4]. This alloy has excellent mechanical properties, like high specific strength comparable with high strength steel [5, 6], offering the potential of reducing weights in some applications. However, the wider use of AA7075-T6 is limited by two main factors: the susceptibility to localized corrosion and the poor tribological properties due to its relatively low hardness and high tendency to adhesion [7, 8].

Many researchers have studied the localized corrosion of AA7075-T6 [7, 9–12]. The susceptibility, to localized corrosion, like pitting, intergranular, or exfoliation corrosion, is related to the type, concentration, and distribution of intermetallics and strengthening particles. These intermetallics and particles have different electrochemical reactivity than the matrix, which could lead to localized galvanic corrosion [13]. The intermetallics and strengthening particles have been characterized with techniques like scanning Kelvin probe force microscopy (SKPFM) or micro-capillary studies [14–17]. In AA7075-T6, Al7Cu2Fe and (Al,Cu)6(Fe,Cu) are the main intermetallics, which are electrochemically less active than the matrix, and therefore they could lead to the dissolution of the surrounding areas [12]. The main strengthening particles contain MgZn2 and the size is in the range of nanometers. These particles precipitate, during heat treatment or aging, along grain boundaries. They are electrochemically more active than the matrix, and thus, they may lead to the intergranular corrosion of AA7075-T6 [7].

In addition to the research of the corrosion properties, the tribological properties of AA7075-T6 have also been studied [8, 18]. In those studies, the effects of surface treatment like plasma electrolytic oxidation or ion implantations on the wear properties of AA7075-T6 have been reported. G. Sabatini et al. reported that plasma electrolytic oxidation treated AA7075-T6 has a significant increase in wear resistance with respect to the base mate-

rial [8]. M.J. Cristobal et al. concluded that the dominant wear mechanism of AA7075-T6 is adhesive-abrasive and this mechanism is not modified by the implantation process [18].

However, in some applications, like slurry transport, aluminum alloys are subject to combined corrosion and abrasion, and the two processes may enhance each other, leading to early material failure. The mechanism of combined corrosion and wear, also known as tribocorrosion, is complex, involving mechanical, chemical and electrochemical factors [19, 20]. For AA7075-T6, the mechanism of combined corrosion and abrasion is rarely understood and this work studies it in detail.

In this chapter, the wear mechanism of combined corrosion and abrasion of aluminum alloy 7075-T6 is presented. A modified pin on disc tribometer, connected with a potentiostat, is used in order to impose intended corrosion conditions. Open circuit potential (OCP), anodic and cathodic potentials are applied. Wear experiments are performed under combined mechanical and (electro)chemical conditions, by means of electrochemical techniques and friction control.

2.2. Experimental

2.2.1. Material preparation

The material, AA7075-T6, was cut to cylinders with 30 mm diameter and 8 mm thickness, to fit the holder of the pin-on-disc tribometer. The main composition of the material is: Al 89.665%, Zn 5.363%, Mg 2.55%, Cu 1.719%, Cr 0.244%, Fe 0.184%, Si 0.115%. After cutting, all the samples were sanded and polished using silicon carbide sandpaper (up to 2400-mesh) and diamond containing polishing liquid (down to 1 μm), respectively, until the finish was mirror-like. Before experiments, samples were cleaned in an ultrasonic bath in acetone to degrease, followed by rinsing and drying.

During experiments, an alumina ball, with 6 mm diameter, was used as the counterpart. After each experiment, the ball was either rotated or replaced to assure fresh and similar contact at the beginning of each experiment.

2.2.2. Tribocorrosion experiment

Tribocorrosion experiments, performed with pin-on-disc tribometry, consisted of two series with different methods to vary the corrosive conditions: chemically by using different liquids and electrochemically by using a potentiostat in 3.5% NaCl solution. For both conditions, the load was 8N and the radius was 5 mm. In the chemical setup, rotational speed was varied from 0.25 to 2.5 Hz (corresponding to 15rpm to 150rpm) and time was varied from 1 to 25 minutes. Three liquids were used: ethanol, deionized water and 3.5% NaCl solution (mimicking the typical chlorine concentration of sea water, and henceforward referred to as sea water) to provide non-corrosive, slightly corrosive and strongly corrosive environments, respectively. In the electrochemical setup, a three-electrode cell configuration potentiostat (Autolab) was connected with the pin-on-disc tribometer. In the three-electrode system, the sample acted as the working electrode, and the counter and reference electrodes were graphite and Ag/AgCl, respectively. Additionally, the pin and the sample holder, both originally made of aluminum, were replaced by plastic ones to avoid possible electrical leakage and stray currents. All the electrochemical experiments were performed in sea water. Before applying a certain potential, the open circuit potential (OCP) was measured. Relative to OCP, potentials in both cathodic and anodic domains were applied. Specifically, -0.5V and -1.0V, relative to OCP, were applied to shift the potential cathodically vs OCP, in order to suppress corrosion. On the other hand, 0.2V and 0.5V, relative to OCP, were chosen to shift the potential anodically vs OCP, in order to accelerate the corrosion. Before the start of sliding, each sample was immersed in sea water at the applied potential for 180 seconds, and thereafter the pin was put in the liquid for another 120

seconds, followed by 300 laps (10 minutes) of sliding with 30 rpm in speed. After the end of sliding, the pin stayed in contact with the sample for 120 seconds before lifted. The total time of each electrochemical experiment was 18 minutes (1080 seconds). Each test was repeated three times to assure reproducibility. The mean value and standard deviation was calculated and reported to compare groups of data.

2.2.3. Characterization

After the tribocorrosion experiments, the wear track profiles were measured by white light interferometry. The wear rate was calculated by multiplying the area of the cross section by the perimeter of the wear track, and then divided by sliding distance [21]. Additionally, Scanning Electron Microscopy (SEM) was used to observe and analyze corrosion morphologies. Multiple locations of the worn and unworn areas were observed by SEM from various magnifications to assure the representativeness. Energy Dispersive X-Ray Spectroscopy (EDS) was used to analyze the chemical composition of particles and corrosion products at the worn and unworn areas.

2.3. Results

2.3.1. Wear response in various corrosive environments

The sample wears the most in sea water, the least in ethanol and the intermediate in deionized water, regardless of rotational speed (Figure 2.1(a)) or time duration (Figure 2.1(b)),. In sea water and ethanol, wear rate remains stable regardless of speed or time duration. For deionized water, at lower rotational speed (0.25 and 0.5Hz), i.e., longer time intervals, the wear rate is larger than that at higher rotational speed. Figure 2.2 shows the relationship between wear rate and electrochemical potentials in sea water. The OCP was measured as -0.68V relative to Ag/AgCl reference electrode. In

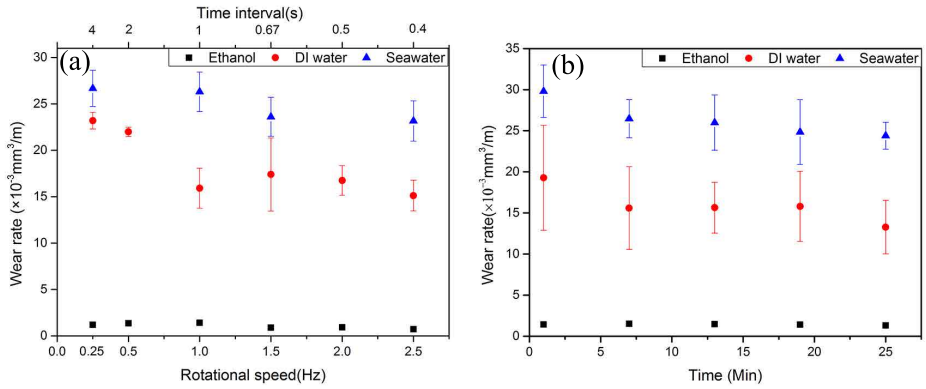

Figure 2.1: (a) Wear rate as a function of rotational speed. The distance was 300 laps for each rotational speed (b) wear rate as a function of time duration. The rotational speed was 1Hz. The load and radius were 8N and 5 mm for all experiments, respectively.

the anodic domain, as shown in Figure 2.2, the sample wears much more than in the cathodic domain, as well as at OCP. Additionally, when applying a higher potential, in the anodic domain, wear rate increases. At OCP, -0.68V, wear rate is roughly 0.026 mm^3/m; when increasing the potential by 0.2V to -0.48V, wear rate increases sharply to 0.053 mm^3/m, twice the rate at OCP; when applying an even higher potential at -0.18V (0.5V relative to OCP) wear rate increases to 0.067 mm^3/m. In the cathodic domain, both at -1.68V (-1.0V vs OCP) or -1.18V (-0.5V vs OCP), wear is comparable with the wear at the OCP.

2.3.2. Surface morphology after experiments at various potentials

The morphology of the unworn area of the samples subjected to various potentials was observed by SEM as shown in Figure 2.3. Grain boundaries are clearly visible as can be seen in Figure 2.3(a), indicating the occurrence of intergranular corrosion at -1.68V (-1.0V vs OCP). Figure 2.3(b) shows local trenching, suggesting the occurrence of pitting corrosion, at -1.18V (-0.5V vs

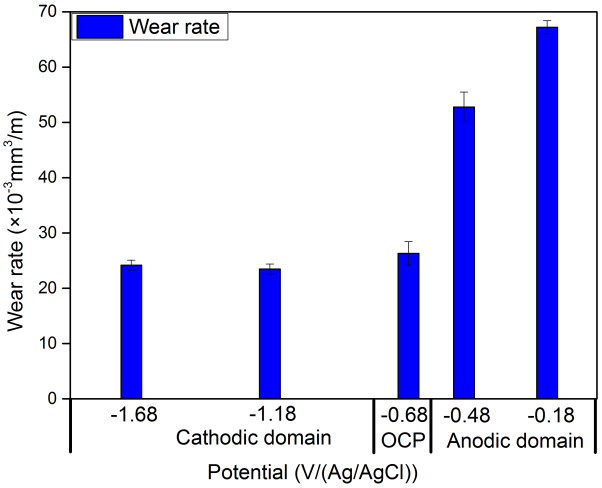

Figure 2.2: Wear rate at various potentials. All potentials were relative to Ag/AgCl standard electrode.

OCP). At the OCP (Figure 2.3(c)), localized trenching and corrosion products were visible. In the anodic domain, the unworn area of the samples showed more corrosion products, as can be seen Figure 2.3(d)(e), representing the occurrence of uniform corrosion at -0.48V (0.2V vs OCP) and -0.18V (0.5V vs OCP). EDS analysis showed that the corrosion products contain Al, Mg, Zn and a large amount of O. The worn area morphology of the samples subjected to various potentials was shown in Figure 2.4. When subjected to the cathodic potential regime, as shown in Figure 2.4(a)(b), the wear mechanism is mainly plastic deformation. Specifically, at -1.68V (-1V vs OCP), ploughed grooves are clearly visible, as shown in Figure 2.4(a); at -1.18V (-0.5V vs OCP), as shown in Figure 2.4(b), wedges appears in addition to grooves. At the OCP (Figure 2.4(c)), both grooves and wedges are visible in the worn area, as well as few corrosion products. In the anodic domain, specifically at -0.48V (0.2V vs OCP) and -0.18V (0.5V vs OCP), the wear mechanism changed drastically. As can be seen in Figure 2.4(d)(e), fewer grooves appeared, but more corrosion products were visible. The chemical

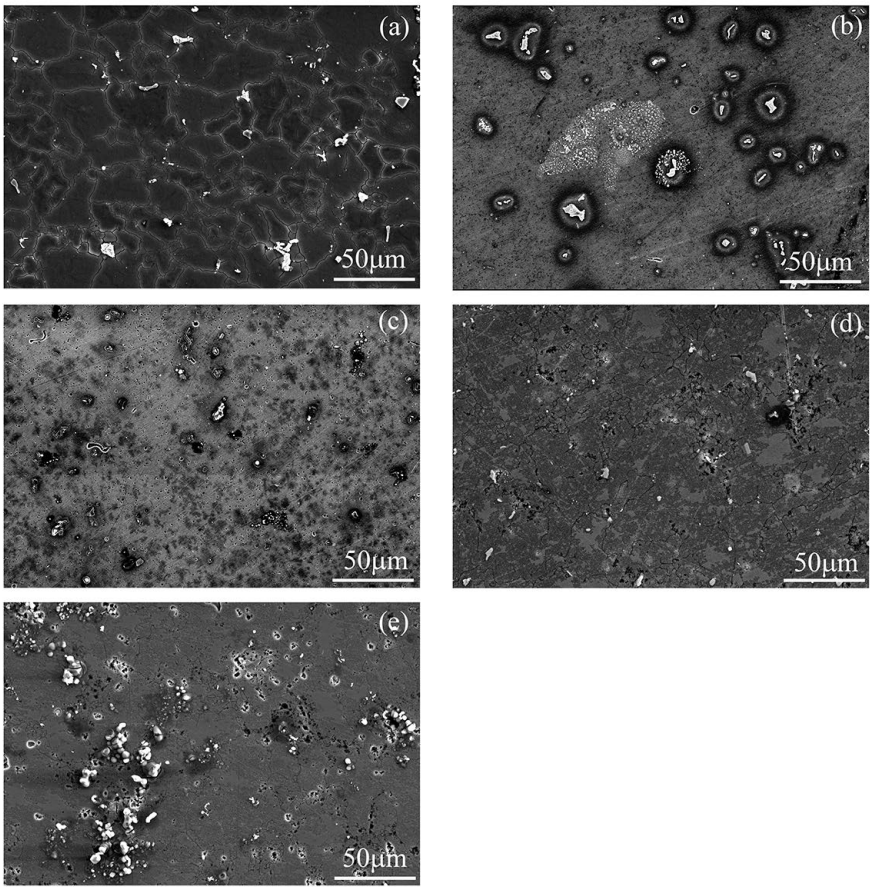

Figure 2.3: Surface morphology of unworn areas after tribocorrosion at different potentials. (a) at -1.68V; (b) at-1.18V; (c) at -0.68V, i.e. OCP; (d) at -0.48V; (e) at -0.18V. All potentials were relative to Ag/AgCl standard electrode. Since the OCP was -0.68V, the five potentials were -1.0, -0.5, 0.0, +0.2 and +0.5V relative to the OCP, respectively. The secondary electron imaging was conducted at acceleration voltage 10kV and the distance was 10 mm.

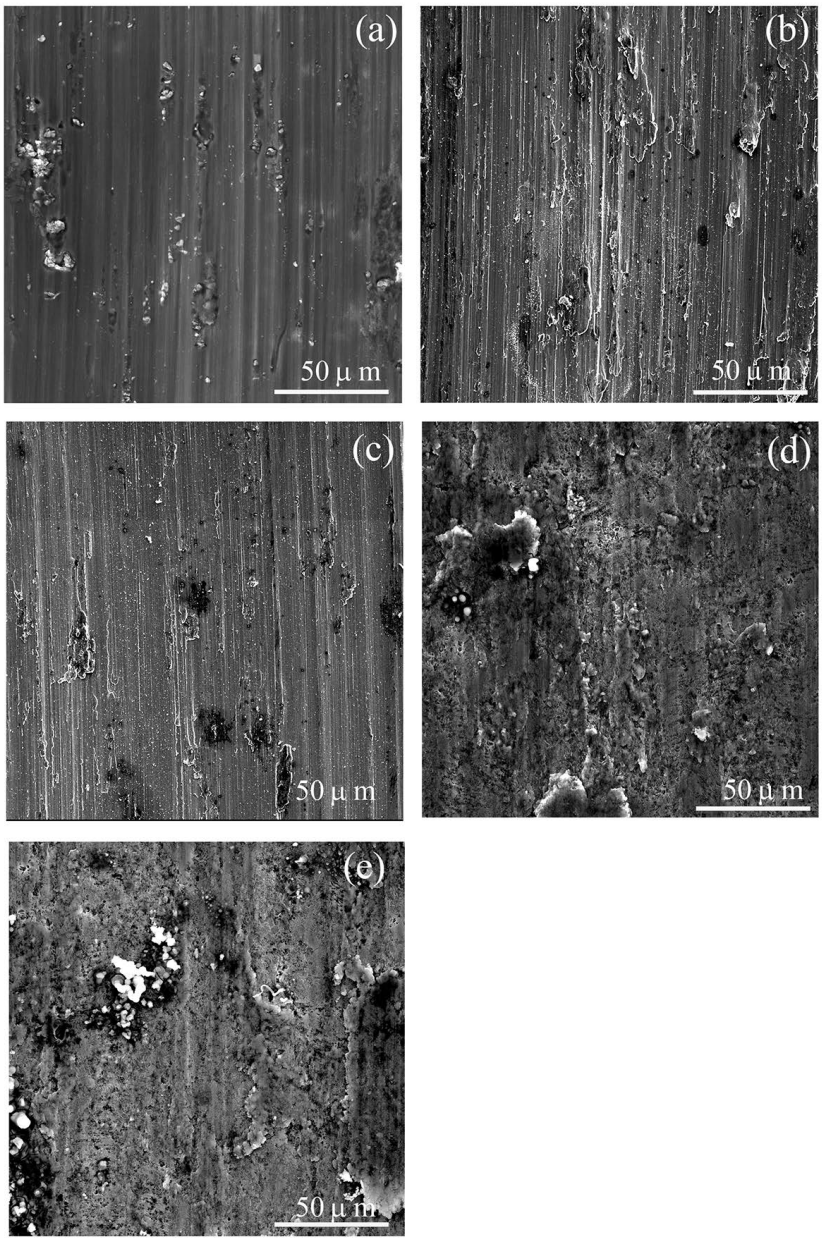

Figure 2.4: Surfaces morphology of worn areas of samples subjected to different potentials. (a) at -1.68V; (b) at-1.18V; (c) at -0.68V, i.e. OCP; (d) at -0.48V; (e) at -0.18V. All potentials were relative to Ag/AgCl standard electrode. Since the OCP was -0.68V, the five potentials were -1.0, -0.5, 0.0, +0.2 and +0.5V relative to the OCP, respectively. The secondary electron imaging was conducted at acceleration voltage 10kV and the distance was 10 mm.

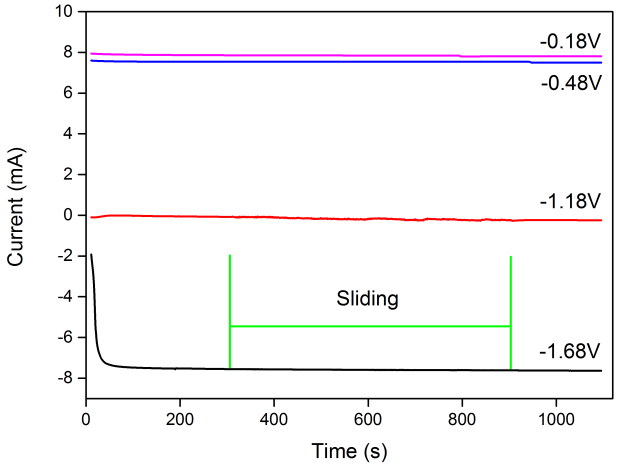

Figure 2.5: The current evolution of the samples as a function of time at various potentials; All potentials were relative to Ag/AgCl standard electrode. Since the OCP was -0.68V, four potentials were -1.0, -0.5, +0.2 and +0.5V relative to the OCP, respectively. The start (300s) and end (900s) of sliding are indicated.

composition of the products at the worn area was similar to that at the unworn area. (Detailed EDS results can be found in appendix A)

2.3.3. Current evolution at various potentials

The current evolution with time at various potentials shows the influence of imposed potential on the current, subsequently corrosion (Figure 2.5). In the cathodic domain, both at -1.68V (-1.0V vs OCP) and -1.18V (-0.5V OCP), the current was negative, indicating that no uniform corrosion on the whole surface occurred. Specifically, at -1.68V, the current (-7.5 mA) was more negative than the current at -1.18V (slightly below zero). In the anodic domain, the current at -0.18V (7.84±0.06mA) was, on average, 4.7% larger than the current at -0.48V (7.49±0.01mA), indicating higher corrosion rate at higher potential in the anodic potentials regime. For both anodic potentials, the positive corrosion current should lead to corrosion products

on the surfaces of samples, as indeed observed on both unworn areas and worn areas, shown in Figure 2.3(d)(e) and Figure 2.4(d)(e), respectively.

2.4. Discussion

AA7075-T6 exhibits various types of corrosion; uniform corrosion, intergranular corrosion, and pitting corrosion. in different corrosive environments [11, 22, 23]. The samples show much higher wear rate in corrosive liquid (sea water) than in non-corrosive liquid (ethanol) (Figure 2.1), suggesting that corrosion increases wear rate. In deionized water, the wear rate was higher at the low rotational speed (0.25 and 0.5Hz) than at the higher rotational speed. At lower speed, the sample has a longer time interval to corrode, and more corrosion products can be removed by subsequent sliding, a process involving repassivation and depassivation [24]. This explains the higher wear rate at lower speed in deionized water. At different rotational speeds in sea water, no noticeable difference can be observed, as shown in Figure 2.1. This might be because the corrosion rate of AA7075-T6 in sea water is too fast for rotational speeds in the range of 0.25-2.5 Hz to make a difference [3].

Corrosion rate is generally determined by the current of the sample according to Faraday's law [25, 26]. In this study, the current at -0.18V (7.84±0.06 mA) was, on average, 4.7% larger than the current at -0.48V (7.49±0.01 mA) (Figure 2.5), indicating that the corrosion rate at -0.18V is higher than that at -0.48V by the application of a higher anodic overpotential. The higher corrosion rate corresponds to the higher wear rate, and this is in agreement with the result that the wear rate in sea water is higher than that in ethanol and deionized water since sea water is the most corrosive one among the three liquids.

When applying a potential in the cathodic domain, corrosion is, in general, suppressed [27, 28]. However, AA7075-T6, only uniform corrosion can be

suppressed, relatively mild localized corrosion still occurs. After the experiment at -1.18V (-0.5V vs OCP), trenching was visible on the surface of the sample (Figure 2.3(b)). The formation of trenching is generally determined by the presence of intermetallics. These intermetallics have different electrochemical potentials relative to the matrix according to the work of Birbilis, et al., who summarized the electrochemical nature of the intermetallics family of AA7075-T6 [10, 29]. The intermetallics and their surrounding areas may form micro-galvanic cells, leading to the formation of trenching [9, 10], as observed and shown in Figure 2.3(b). The occurrence of trenching implies the existence of localized corrosion, and the wear rate at -1.18V is still comparable with the wear rate at the OCP (Figure 2.2), suggesting that localized corrosion is the reason that the wear rate at -1.18V (in the cathodic domain) does not drop noticeably. At -1.68V, mild intergranular corrosion appeared along grain boundaries as shown in Figure 2.3(a). In AA7075-T6, the main precipitations of the strengthening particles contain MgZn2 [7]. These precipitations can create an anodic path for the localized attack along grain boundaries due to their extremely low electrochemical potential [29], leading to the intergranular corrosion [7, 9]. In this study, intergranular corrosion occurred at -1.68V (-1.0V vs OCP), and the wear rate was still comparable with the wear rate at the OCP (Figure 2.2), suggesting that intergranular corrosion is the reason that the wear rate at -1.68V (in the cathodic domain) does not drop noticeably. In the anodic domain, as shown in Figure 2.3(d)(e), intergranular corrosion, local attack and uniform corrosion were all visible. Besides, in the anodic domain, more generation of gas than at the OCP was observed, indicating the higher intensity of corrosion reaction.

2.5. Conclusions

The combined corrosion and wear of AA7075-T6 was studied. Wear rate was much higher in sea water than in deionized water and ethanol, because

of the high corrosion rate in sea water and the easy removal of corrosion products by subsequent sliding movement. When applying anodic potentials to accelerate corrosion rate, the wear rate became higher than that at OCP, further confirming that the higher corrosion rate leads to the higher wear rate of AA7075-T6 due to the formation and removal of corrosion films during tribocorrosion. When applying cathodic potentials on the sample in sea water, wear rate did not drop noticeably compared to the condition at the OCP. This is due to the occurrence of mild intergranular corrosion caused by strengthening precipitation particles, or localized corrosion caused by intermetallics.

References

[1] W. Miller, L. Zhuang, J. Bottema, A. Wittebrood, P. De Smet, A. Haszler, and A. Vieregge, *Recent development in aluminium alloys for the automotive industry,* Materials Science and Engineering: A **280**, 37 (2000).

[2] R. L. Deuis, C. Subramanian, and J. M. Yellupb, *Dry Sliding Wear of Aluminium Composites-a Review,* Composites Science and Technology **57**, 415 (1997).

[3] C. Vargel, *Corrosion of Aluminium* (Elsevier Ltd, Oxford, 2004).

[4] E. Starke and J. Staley, *Application of modern aluminum alloys to aircraft,* Progress in Aerospace Sciences **32**, 131 (1996).

[5] S. W. Lee, J. W. Yeh, and Y. S. Liao, *Premium 7075 aluminium alloys produced by Reciprocating extrusion,* Advanced Engineering Materials **6**, 936 (2004).

[6] D. Liu, H. V. Atkinson, P. Kapranos, W. Jirattiticharoean, and H. Jones, *Microstructural evolution and tensile mechanical properties of thixoformed high performance aluminium alloys,* Materials Science and Engineering A **361**, 213 (2003).

[7] F. Andreatta, H. Terryn, and J. de Wit, *Corrosion behaviour of different tempers of AA7075 aluminium alloy,* Electrochimica Acta **49**, 2851 (2004).

[8] G. Sabatini, L. Ceschini, C. Martini, J. A. Williams, and I. M. Hutchings, *Improving sliding and abrasive wear behaviour of cast A356 and wrought AA7075 aluminium alloys by plasma electrolytic oxidation,* Materials and Design **31**, 816 (2010).

[9] F. Andreatta, M. M. Lohrengel, H. Terryn, and J. H. W. De Wit, *Electrochemical characterisation of aluminium AA7075-T6 and solution heat*

treated AA7075 using a micro-capillary cell, Electrochimica Acta **48**, 3239 (2003).

[10] N. Birbilis, M. K. Cavanaugh, and R. G. Buchheit, *Electrochemical behavior and localized corrosion associated with Al7Cu2Fe particles in aluminum alloy 7075-T651,* Corrosion Science **48**, 4202 (2006).

[11] U. Zupanc and J. Grum, *Effect of pitting corrosion on fatigue performance of shot-peened aluminium alloy 7075-T651,* Journal of Materials Processing Technology **210**, 1197 (2010).

[12] M. Gao, C. R. Feng, and R. P. Wei, *An analytical electron microscopy study of constituent particles in commercial 7075-T6 and 2024-T3 alloys,* Metallurgical and Materials Transactions A: Physical Metallurgy and Materials Science **29**, 1145 (1998).

[13] P. S. Pao, C. R. Feng, and S. J. Gill, *Corrosion fatigue crack initiation in aluminum alloys 7075 and 7050,* Corrosion **56**, 1022 (2000).

[14] H. Böhni, T. Suter, and F. Assi, *Micro-electrochemical techniques for studies of localized processes on metal surfaces in the nanometer range,* Surface and Coatings Technology **130**, 80 (2000).

[15] M. M. Lohrengel, A. Moehring, and M. Pilaski, *Capillary-based droplet cells: Limits and new aspects,* Electrochimica Acta **47**, 137 (2001).

[16] P. Schmutz, *Corrosion Study of AA2024-T3 by Scanning Kelvin Probe Force Microscopy and In Situ Atomic Force Microscopy Scratching,* Journal of The Electrochemical Society **145**, 2295 (1998).

[17] P. Schmutz, *Characterization of AA2024-T3 by Scanning Kelvin Probe Force Microscopy,* Journal of The Electrochemical Society **145**, 2285 (1998).

[18] M. Cristóbal, R. Figueroa, L. Mera, and G. Pena, *Tribological behaviour of aluminium alloy AA7075 after ion implantation,* Surface and Coatings Technology **209**, 124 (2012).

[19] P. Ponthiaux, F. Wenger, D. Drees, and J. P. Celis, *Electrochemical techniques for studying tribocorrosion processes,* Wear **256**, 459 (2004).

[20] D. Landolt, *Electrochemical and materials aspects of tribocorrosion systems,* Journal of Physics D: Applied Physics **39**, 3121 (2006).

[21] E. Rabinowicz, *Friction and Wear of Materials(2nd edition)* (J. Wiley, 1995).

[22] J. feng LI, Z. wei PENG, C. xing LI, Z. qiang JIA, W. jing CHEN, and Z. qiao ZHENG, *Mechanical properties, corrosion behaviors and microstructures of 7075 aluminium alloy with various aging treatments,* Transactions of Nonferrous Metals Society of China (English Edition) **18**, 755 (2008).

[23] R. Y. Hwang and C. P. Chou, *Corrosion behaviour of weld heat affected zone of aluminium alloy 7075,* Science and Technology of Welding and Joining **2**, 269 (1997).

[24] D. Landolt, S. Mischler, and M. Stemp, *Electrochemical methods in tribocorrosion: A critical appraisal,* Electrochimica Acta **46**, 3913 (2001).

[25] R. G. Ehl and A. J. Ihde, *Faraday's electrochemical laws and the determination of equivalent weights,* Journal of chemical education **31**, 226 (1954).

[26] F. C. Strong, *Faraday's laws in one equation,* Journal of Chemical Education **38**, 98 (1961).

[27] P. Pedeferri, *Cathodic protection and cathodic prevention,* Construction and Building Materials **10**, 391 (1996).

[28] V. Ashworth, *Principles of cathodic protection,* Shreir's Corrosion **4**, 2747 (2010).

[29] N. Birbilis and R. G. Buchheit, *Electrochemical Characteristics of Intermetallic Phases in Aluminum Alloys,* Journal of The Electrochemical Society **152**, B140 (2005).

3

Roughness as an indicator of wear in slurry loop experiments

Keep your eyes on the stars and your feet on the ground

Theodore Roosevelt

This chapter is based on the following article:

E. A. Chemmalasseri*, Yueting Liu*, A.M. Talmon, G. Palasantzas, G.C.A.M. Janssen, C. van Rhee. Roughness as an indicator of wear in slurry loop experiments (submitted to Materials)

* These authors contributed equally to this article

3

This chapter presents the wear study in a slurry loop. A 55-meter long slurry loop with controlled flow conditions was employed to mimic, in the laboratory, the situation of actual slurry transport. Two liquids were used, namely fresh water and sea water, to study the influence of corrosion on the wear of the pipes. Two types of particles were used with a difference in size to investigate the effect of particle size. For each set of experiments, three coupons were placed on the top, side, and bottom of the wall, and the coupons were aligned nominally flush with the wall. The results show that the roughness across the worn sample is, in some cases, highly non-uniform. The misalignment is responsible for the non-uniform roughness profile, and the roughness profile, in turn, implies a non-uniform wear. These findings suggest that sample size, flush mounting and wear measurement are critical to study wear in slurry loop, and roughness is a useful indicator of wear.

3.1. Introduction

Hydraulic transport through pipelines is efficient in the fields of mining and dredging. From the 1940s papers have appeared on slurry transport, followed by numerous studies on the design and efficacy of the systems [1–3]. However, the limited lifespan of the slurry pipes is still a huge problem. The lifespan is largely limited by erosive wear, mainly due to sliding and impacting of the particles on the pipe walls. Corrosion also plays a role when the liquid is corrosive, and the synergism between wear and corrosion may further exacerbate the problem leading to early failure of the pipes, and therefore to high maintenance costs [4–6].

The main factors that determine wear rate of slurry pipelines are the properties of the slurry itself, the properties of the pipe materials and the nature of the fluid flow [7]. The properties of slurry mainly include the particle hardness, size, shape (sharpness), specific mass, and concentration. The properties of materials mainly include chemical composition, microstructure, and hardness. Finally, the mode of flow in principle determines the particle dispersion and particle motion, which eventually determine the wear mechanism.

Various techniques have been used to study the wear mechanism by mimicking the conditions during slurry transport in the lab. Some techniques focus on the impacting effect like gas-blast and centrifugal-accelerator erosion testers. A detailed comparison of these two methods pointed out that the results for gas-blast testers are sensitive to both the particle velocity and the dispersion. Centrifugal accelerator erosion testers provide closer control of the important parameters, but it requires an account for erosion effects associated with the impact of rotating particles, an inherent feature of this tester [8]. Slurry pot is another common erosion tester featuring erosion corrosion environment. Notably, a number of Dutch dredging and offshore companies, in cooperation with Dutch Applied Scientific Organi-

zation TNO, performed a three-year project using slurry pot, studying the corrosion-erosion in coal slurries [9]. A series of parameters such as erosion angle, speed, and particle size were varied to study the influence on wear, and eventually a relative index of erosion resistance was obtained. Several erosion testers, featuring sliding wear, have been used as well like Wet Sand/Rubber Wheel Abrasion Tester and Coriolis erosion tester. Wet Sand/Rubber Wheel Abrasion Tests is a standard test method of ASTM(ASTM G105 - 02(2007)), useful to perform abrasive and corrosive wear test. Coriolis erosion tester was introduced originally by Tuzson in 1984, featuring the interaction between the dense slurry and the targeted surfaces like the pumps or pipelines [10]. In addition to the various apparatus, modeling on erosion is a technique that aims to simulate the process and predict material loss, as reported by researchers [11, 12].

In slurry transport field tests, the particles in the slurry tend to settle down due to gravity, depending on the particle size and flow properties. The slurries tend to be heterogeneous, and typically stratified [13–15]. To overcome the limitations of the test mentioned above and to mimic as close as possible the real situation, a 55-meter long slurry loop with controlled flow conditions was employed. The idea is to mount a test coupon flush with the wall of the slurry loop at the top, the bottom, and the side position and to study the wear of this coupon after hours-long test with specified particles, dilution and flow velocity. Additionally, the salinity of slurry has a strong influence on corrosivity, and therefore the wear mechanism of slurry pipes. However, the comparison of wear rate in liquids with different salinity is rarely reported. The main findings of this study are twofold. Firstly, the method to know the position of the unworn surface of the coupon after the experiment was not successful. Moreover, in a number of experiments, the roughness of the coupon was uniform over the sample while in other cases the roughness was extremely non-uniform.

3.2. Experimental

3.2.1. Slurry loop and the sample preparation

The 150 mm diameter test circuit in the laboratory of the Dredging engineering section of Delft University of Technology was used to conduct the experiment. The test circuit was observed to produce measurable wear on a test coupon and hence, deemed useful to conduct wear tests. The schematic diagram of the slurry test circuit is shown in Figure 3.1. The detailed description of this test circuit was given by Matousek [16]. Later the details of the setup were modified by van Rhee [17]. This study used the modified version. The sample and the positioning are shown in Figure 3.2. The sample was a coupon, made of structural steel based on the European standard EN10025. It is 150 mm in length and 10 mm in width. The coupon can be easily dismounted and replaced. A part of the coupon is isolated from the flow using a bolt to serve as a reference surface for wear profile measurement using white light interferometer [18]. With this setup, it is possible to study the circumferential distribution of wear in pipes, about which very little information is available [12]. Flow regimes and particle size distribution can be varied. In this first series the parameters were restricted to a flow speed of 5 m/s, a sand concentration of 20%, artificial sea water and fresh water.

3.2.2. Experimental procedure

Prior to mounting, the surface of the coupon was finely polished (until a mirror-like surface) using a mechanical polishing machine. Two different sizes of dorsilit crystal quartz sands were used for the experiments. Dorsilit 8 and Dosilit 7 have grain diameters of 0.3-0.8 mm and 0.6-1.2 mm respectively. After polishing, the coupons are mounted on a section of pipe in the slurry loop as shown in Figure 3.2. The coupons were aligned nominally flush with the wall and with a bolt protecting the reference area, to mark

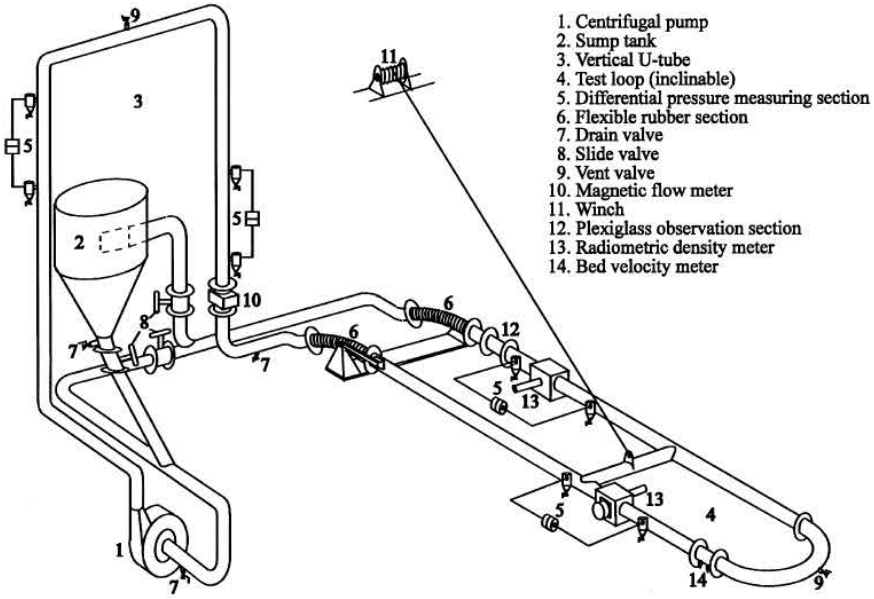

Figure 3.1: Schematic diagram of the slurry test circuit.

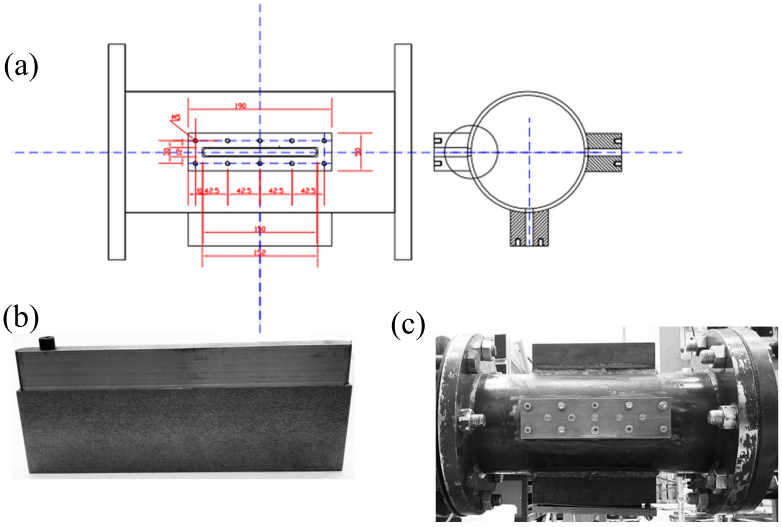

Figure 3.2: Sample and the sample positioning. (a) shows the positioning of the sample; (b) shows the sample with a bolt on the left; (c) shows the position of the loop where the sample was placed.

the position of the unworn sample surface at the downstream end of the coupon. This position was chosen to prevent any disturbance in the flow over the wear coupon. To simulate conditions in dredging projects, artificial sea water, in comparison with fresh water, was created by mixing about 3.5% by weight of sodium chloride (industrial salt). Sand concentration of 20 percent (by volume) was introduced into the slurry loop. Subsequently, the sand-water mixture and fresh water were circulated in the pipe loop at an average flow velocity of 5m/s, respectively. The flow regime was visually observed through the transparent window made of lexan and no stationary bed layer was seen. The mixture was circulated through the slurry loop for 5 hours. After the experiment, the pipe section containing the coupons was isolated using valves, and the water inside was drained to remove the wear coupons.

3.3. Results

3.3.1. Worn surface profile and roughness calculation

The worn surface of the sample is shown in Figure 3.3(a). The color is an indication of the height, and thereby the wear. The bolt downstream at the left created vortices in the flow close to it. In some cases, a step between the part covered by the bolt-head and the uncovered part of the coupon was visible, but not in all cases. Moreover, it turned out to be a cumbersome problem to decide on the position of the unworn surface based on a single height measurement on one side of the wear coupon. To analyze our data the roughness over the length of the coupon was measured. Roughness was measured along 10 mm long line scans. These scans were done along the centerline of the sample, i.e., from 25 mm to 35 mm, from 35 mm to 45 mm etc. Also 10 mm long scans were made over the width of the sample at positions increasing by 10 mm each time. Figure 3.3b shows all 10 mm long scans, which were used to determine the roughness. The

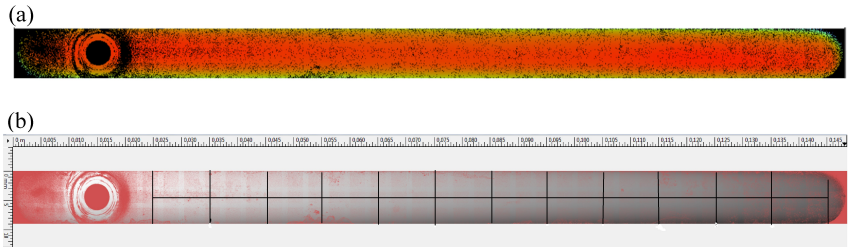

Figure 3.3: Worn surface and roughness analysis. (a) shows the worn morphology of the sample after wear in slurry loop; (b) shows the roughness analysis along both flow direction (horizontal) and the perpendicular direction (vertical). The total length of the analysis is from the position of the bolt to the right end of the surface.

total analysis area is from the position of the bolt to the right end. The roughness in this paper is the root mean square: RMS: the overall deviation from the mean curve. The mean curve is chosen in such a way that the residuals above and below the mean line have the same area. The mean curve is a piecewise continuous function with a curvature up to the cutoff frequency. The cutoff, that separates waviness from roughness, has been kept constant for all measurements at 1% of Nyquist frequency [19, 20]. With this cut-off frequency, the initial surface curvature, before experiments, is categorized as waviness, and therefore the initial roughness is negligible. Any wavelength larger than the cutoff wavelength is considered waviness and therefore removed from the primary surface texture. The residual peaks and valleys above and below the waviness profile make up of roughness profile.

The roughness (RMS) is, segmentally, calculated along both the horizontal and vertical directions of the worn surface (Figure 3.3 illustrates the lines). The horizontal roughness is, segmentally, calculated along the middle line between 25-145 mm of a whole sample size, with 10 mm as increment. Thus, the segments are 25-35 mm, 35-45 mm, ..., 135-145 mm, and in Figure 3.4, they are denoted by the middle points of the segments: 30, 40, ...130, 140. The vertical roughness is calculated along the vertical lines

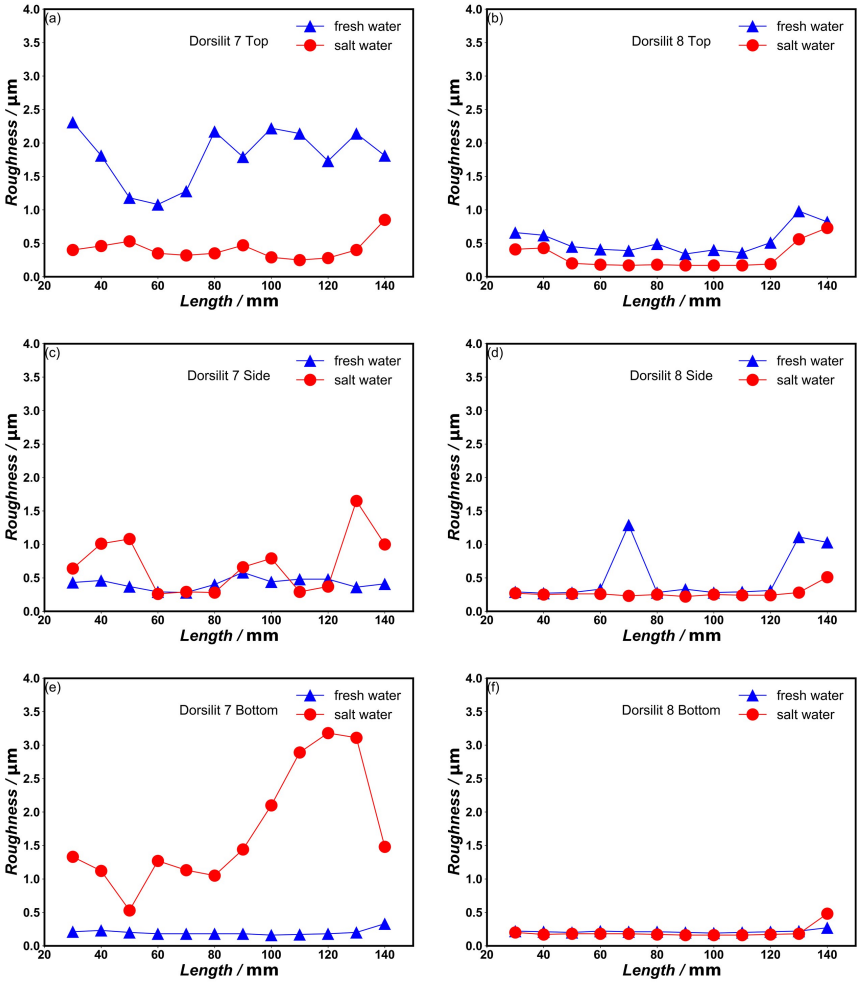

Figure 3.4: Roughness comparison between fresh water and saltwater for all top, side and bottom positions along the flow direction (horizontal). The left three (a)(c)(e) subfigures are roughness results with large particles (Dorsilit 7), while the right three subfigures (b)(d)(f) are roughness results with small particles (Dorsilit 8).

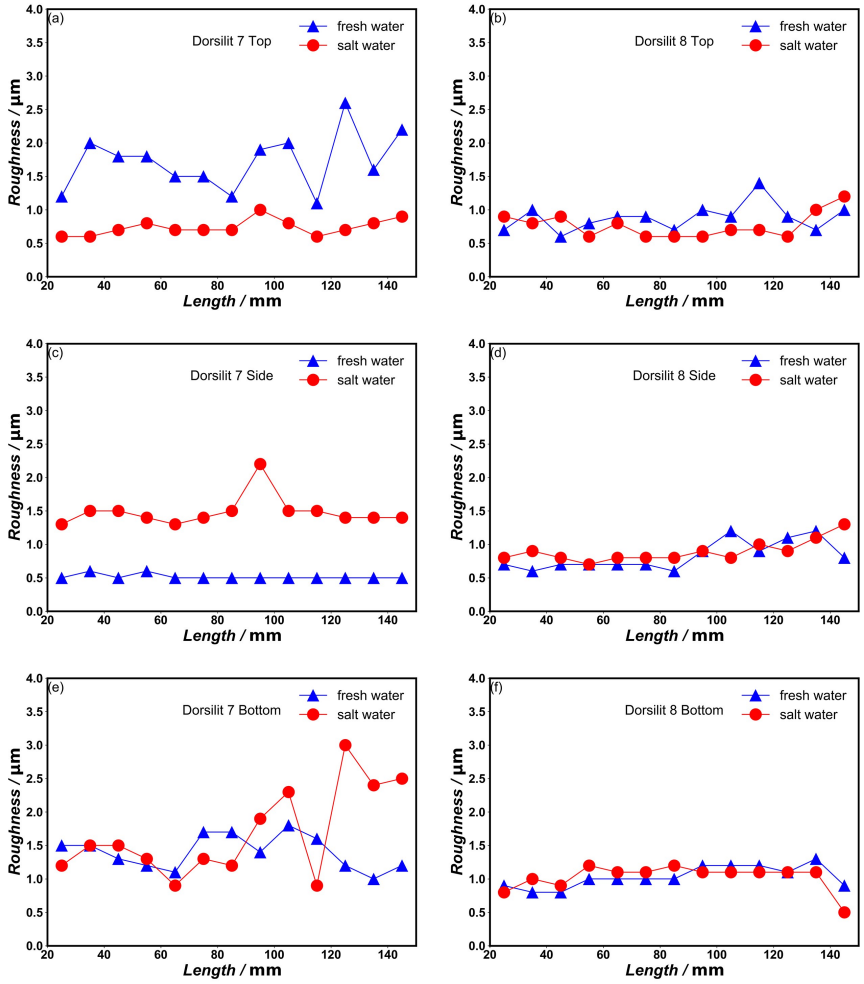

Figure 3.5: Roughness comparison between fresh water and saltwater for all top, side and bottom positions along the perpendicular direction (vertical). The left three (a)(c)(e) subfigures are roughness results with large particles (Dorsilit 7), while the right three subfigures (b)(d)(f) are roughness results with small particles (Dorsilit 8).

from 25-145 mm, also with 10 mm as increment, and in Figure 3.5, they are denoted by the positions of the vertical lines, thus: 25, 35, ..., 135, 145.

3.3.2. Roughness analysis across the worn surface

The roughness of the worn sample, measured along the flow direction is shown in Figure 3.4. On the right side, the results for the smaller particles (Dorsilit 8) show a uniform roughness over the length of the coupon. Also, the roughness for salt water and fresh water is the same for side and bottom, while for the top position the roughness is two times larger for the fresh water experiment. On the left side, the results for the larger particles are presented. Here shows huge differences between fresh water and salt water experiments. For the top position, the fresh water coupon is four times rougher than the salt water coupon. For the bottom position, the salt water coupon is up to fifteen times rougher than the fresh water coupon. The roughness measured along the scans perpendicular to the flow direction (Figure 3.5), shows similar results. For the small particles (Dorsilit 8 right side), the roughness is constant and about the same for fresh water and sea water. Also, no difference based on position in the tube is found. The roughness is about twice as high as the roughness measured on the same coupons in the flow direction. Here again the larger particles (Dorsilit 7) show higher roughness values and sometimes marked differences for fresh water and salt water. For Dorsilit 7 at the top position, roughness is the largest in fresh water, while at the side position roughness is the largest for salt water.

3.4. Discussion

Roughness is a measure of surface topography and researchers found that roughness can be used to compare wear among materials with various hardness [21]. In Figure 3.6, the relation between wear and roughness

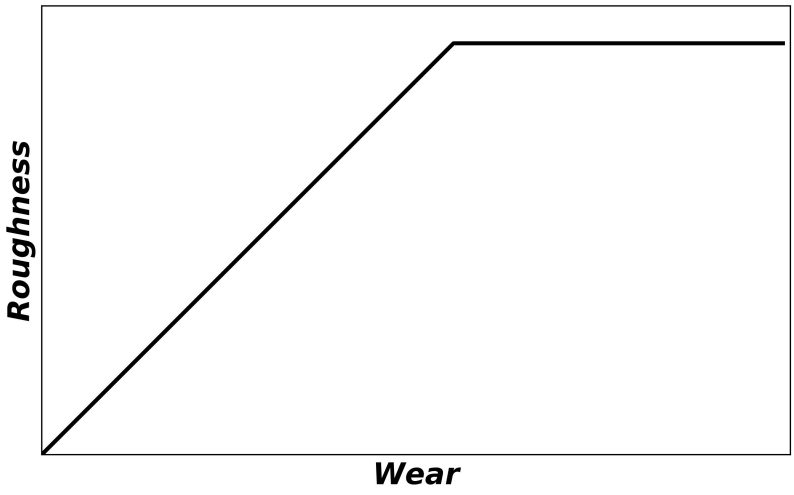

Figure 3.6: A sketch of the relationship between roughness and wear. The initial surface is mirror-like smooth. As wear proceeds, roughness increases until reaching a certain level.

is sketched. Starting from a polished surface abrasive wear will at the same time remove material, i.e. wear, and increase the roughness. When the surface is uniformly worn, the roughness across the surface should be constant. Until the steady state is reached, roughness is a measure for wear. For the small particles (Dorsilit 8), the roughness is uniform both in the flow direction as well as in the direction perpendicular to the flow. Moreover, the roughness in fresh water and salt water is about the same. It should be noted however that the roughness in the perpendicular direction is about a factor of two larger than in the direction parallel to the flow. This factor of two is explained by an edge effect. Closer to the edge of the coupon the wear is more severe and hence the roughness. This shows up in the roughness determined in a perpendicular scan over the total width of the coupon. For the larger particles (Dorsilit 7), the roughness shows differences between salt and fresh water and also non-uniformities over the length of the coupon. The results, obtained for Dorsilit 7, were not due to the flow,

nor the salinity, but due to the non-flush mounting of the coupon.

In the non-uniform worn samples, the roughness difference between salt water and fresh water can be up to a factor of 10. The large differences were caused by the alignment of the wear coupon. In the cases where large roughness, and thereby wear is observed, the coupon was protruding into the flow, leading to extra wear and rougher surface, analogous to the rounding off observed by a carpenter while sanding a flat object of limited length. In the cases of low but uniform roughness, the coupon was either flush with the wall or slightly recessed.

3.5. Conclusions

In this study, the wear of the sample coupons was quantified by the surface roughness. Results show that the roughness of the worn sample varies across the surface, caused by the non-flush mounting of the sample in the slurry loop. Analysis has shown that the roughness across the worn sample surface is, in some cases, highly non-uniform. The coupon misalignment is responsible for the non-uniform roughness profile, and the roughness profile, in turn, implies a non-uniform wear. Given the fact that the surface roughness of the sample can be fully attributed to wear, since the initial roughness of the sample before wear is negligible. Since the roughness profile implies a non-uniform wear, the measurement of the wear values will be highly sample location or size dependent, and are therefore not representative for the slurry loop conditions. These findings suggest that sample size, flush mounting and wear measurement are critical to study wear in slurry loop, and roughness as an indicator of wear is highly useful.

References

[1] L. Suo and E. Wylie, *Complex Wavespeed and Hydraulic Transients in Viscoelastic Pipes,* Journal of Fluids Engineering **112**, 496 (1990).

[2] F. Ravelet, F. Bakir, S. Khelladi, and R. Rey, *Experimental study of hydraulic transport of large particles in horizontal pipes,* Experimental Thermal and Fluid Science **45**, 187 (2013).

[3] P. Doron, D. Granica, and D. Barnea, *Slurry flow in horizontal pipes-experimental and modeling,* International Journal of Multiphase Flow **13**, 535 (1987).

[4] H. M. Clark and R. J. Llewellyn, *Assessment of the erosion resistance of steels used for slurry handling and transport in mineral processing applications,* Wear **250-251**, 32 (2001).

[5] H. M. Clark, J. Tuzson, and K. K. Wong, *Measurements of specific energies for erosive wear using a Coriolis erosion tester,* Wear **241**, 1 (2000).

[6] C. I. Walker and P. Robbie, *Comparison of some laboratory wear tests and field wear in slurry pumps,* Wear **302**, 1026 (2013).

[7] G. Truscott, *A literature survey on abrasive wear in hydraulic machinery,* Wear **20**, 29 (1972).

[8] T. Deng, M. S. Bingley, M. S. A. Bradley, and S. R. De Silva, *A comparison of the gas-blast and centrifugal-accelerator erosion testers: The influence of particle dynamics,* Wear **265**, 945 (2008).

[9] J. W. M. Mens and A. W. J. de Gee, *Erosion in seawater sand slurries,* Tribology International **19**, 59 (1986).

[10] J. J. Tuzson, *Laboratory Slurry Erosion Tests and Pump Wear Rate Calculations,* Journal of Fluids Engineering **106**, 135 (1984).

[11] C. Y. Wong, C. Solnordal, A. Swallow, S. Wang, L. Graham, and J. Wu, *Predicting the material loss around a hole due to sand erosion,* Wear **276-277**, 1 (2012).

[12] R. J. K. Wood, T. F. Jones, J. Ganeshalingam, and N. J. Miles, *Comparison of predicted and experimental erosion estimates in slurry ducts,* Wear **256**, 937 (2004).

[13] A. R. Oroskar and R. M. Turian, *Critical Velocity in Pipeline Flow of Slurries.* AIChE Journal **26**, 550 (1980).

[14] F. J. Pugh and K. C. Wilson, *Role of the interface in stratified slurry flow,* Powder Technology **104**, 221 (1999).

[15] V. Matoušek, *Research developments in pipeline transport of settling slurries,* Powder Technology **156**, 43 (2005).

[16] V. Matoušek, *Pressure drops and flow patterns in sand-mixture pipes,* Experimental Thermal and Fluid Science **26**, 693 (2002).

[17] C. Van Rhee, *On the sedimentation process in a trailing suction hopper dredger*, Phd thesis, Delft University of Technology (2002).

[18] E. Chemmalasseri and A. Talmon, *Characterization of hydro-abrasive wear in the slurry pipelines using white light interferometer,* in *19th International Conference on Hydrotransport* (Colorado, 2014) pp. 315–324.

[19] P. de Groot and L. Deck, *Surface profiling by analysis of white-light interferograms in the spatial frequency domain,* Journal of Modern Optics **42**, 389 (1995).

[20] F. El Feninat, S. Elouatik, T. H. Ellis, E. Sacher, and I. Stangel, *Quantitative assessment of surface roughness as measured by AFM: Application to polished human dentin,* Applied Surface Science **183**, 205 (2001).

[21] V. Jankauskas and R. Skirkus, *Steel abrasive wear forecasting by wearing surfaces microgeometric parameters,* Mechanika **19**, 486 (2013).

4

Corrosion reduces wet abrasive wear of structural steel

Success is a science;
if you have the conditions,
you get the results

Oscar Wilde

This chapter is based on the following article:
Liu, Yueting, J. M. C. Mol, and G. C. A. M. Janssen. "Corrosion reduces wet abrasive wear of structural steel." Scripta Materialia 107, 92 (2015)

4

In this chapter, the wear mechanism of galvanic micro coupling is presented. This mechanism is counter-intuitive and distinct from the mechanism of cyclic formation and removal of surface film, as presented in chapter 2. The abrasive corrosive wear experiments were performed on a structural steel S235, a common used engineering steel. Experiments were performed with a pin on disc tribometer in artificial sea water, deionized water and ethanol. Counterintuitively the wear rate is observed to be the smallest in sea water. The smallest wear rate in sea water is due to the combined chemical modification of the steel surface due to local electrochemical interaction with the sea water and the mechanical interaction between the pin and the surface

4.1. Introduction

Abrasive wear and corrosion are two common materials degradation processes that lead to high costs of maintenance in industries. When the two processes co-exist, a combined effect occurs. As a result of the combined effect, the surface of the material will be progressively removed due to mechanical, chemical/electrochemical processes, and the interaction between these two. The combined effect typically leads to a faster degradation rate of materials than the arithmetic sum of the two components [1].

The combined effect between abrasive wear and corrosion is complex. The knowledge of the two separate processes, i.e., either the tribological behavior in the absence of corrosive environment, or the chemical/electrochemical behavior in the absence of mechanical motion, is not sufficient to derive the final material degradation behavior, as the combined effect plays a impacting role [2].

It has been reported that abrasive wear could modify the sensitivity of the materials to corrosion (e.g., abrasive wear may lead to the destruction of the surface corrosion film, which could further alter the corrosion rate of the material). On the other hand, corrosion could change the wear resistance of the material by modifying the surface (e.g., loose corrosion products may form on the surface of the material which are not as wear resistant as the substrate material) [3]. Due to the interaction between abrasive wear and corrosion, the combined effect of these two processes usually expedites the degradation of the material [4–9]. In an experiment, the amount of material removed by abrasive wear in the absence of corrosion can be estimated (by suppressing corrosion, e.g., applying cathodic protection). The difference between the total wear and abrasive wear can be calculated and the influence of corrosion can, therefore, be quantified.

In this study, a pin on disc tribometer was used to provide the abrasive corrosive experimental environment. various liquids were used to vary corrosion

conditions. Mechanical conditions, like velocities and loads, were varied as well. To elucidate the interaction between abrasion and corrosion, cathodic protection was employed to separate corrosion from abrasion.

4.2. Experimental

4.2.1. Materials

Structural steel S235 was used in this study. According to European Standard EN 10025 [10], structural steel offers a good combination of welding properties with guaranteed strength. S235, with a minimum yield strength of 235 MPa, is extensively used in engineering fields like dredging. The microstructure of S235 steel, shown in Figure 4.1, consists of ferrite and pearlite. The grains size is around 20 µm. Cylindrical samples with a diameter of 30 mm and a thickness of around 8 mm were cut from a steel bar. Before experiments, the samples were sanded using silicon carbide sandpaper up to 2400-mesh and then polished using polishing liquid containing diamond particles up to 1 µm. Finally, the samples were cleaned ultrasonically in acetone followed by rinsing with distilled water and then dried with room temperature air. The counterpart used in this study was an aluminum oxide ball with a diameter of 6 mm. After each experiment, the ball was either rotated or replaced to obtain fresh contact between the sample and the ball.

4.2.2. Corrosive abrasive wear experiments

A rotary pin on disc tribometer with a liquid container was used to conduct abrasive wear experiments. Three liquids were used, namely ethanol, deionized (DI) water and 3.5% NaCl solution to simulate sea water. Loads of 1 N, 2 N, 5 N, and 10 N were applied. These loads correspond to initial maximum Hertzian contact pressure of 432 MPa, 545 MPa, 739 MPa, and 931 MPa. Ve-

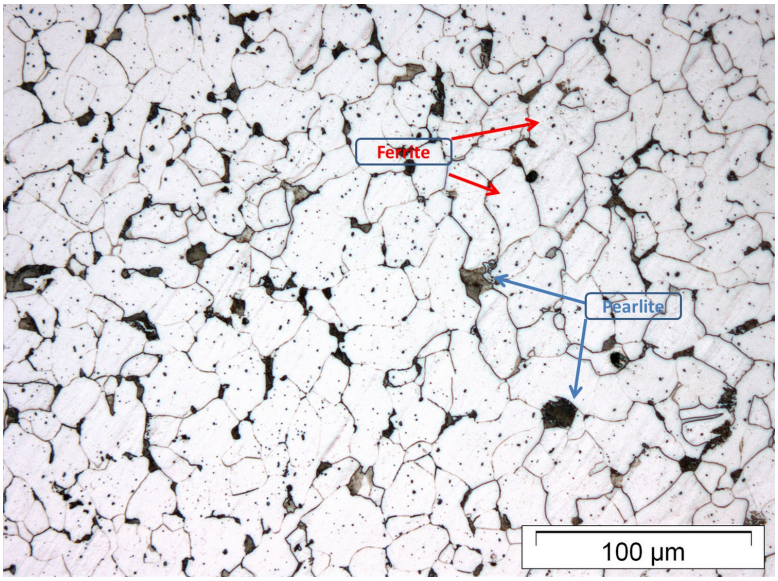

Figure 4.1: Microstructure of the sample. The sample contains mainly ferrite and cementite. The graph was taken with optical microscope. 2% nital was used to etch the surface

locities of 1.25 cm/s, 2.51 cm/s, 5.02 cm/s, 10.04 cm/s, and 15.06 cm/s were used. These velocities were the results of rotational frequencies of 0.25 Hz, 0.5 Hz, 1 Hz, 2 Hz, and 3 Hz. All experiments were conducted at a radius of 8 mm. First the load was varied from 1 N to 10 N with a fixed velocity of 10.04 cm/s, then the velocity was varied from 1.25 cm/s to 15.06 cm/s with a fixed load of 10 N. All experiments were carried out in three liquids. The coefficient of friction(COF) was recorded by the tribometer in real time. After experiments, a White Light Interferometer was used to measure wear track profile. Area of cross section was calculated and eventually converted to wear rate in the unit of mm^3/Nm [11]. Scanning electron microscopy (SEM) was used to observe the morphology of wear tracks.

4.2.3. Immersion experiments in sea water and DI water

Identical samples were immersed in deionized water and sea water respectively for 24 hours, to study the influence of corrosion environment on the surface of the sample. After immersion, SEM was used to observe the surface morphology.

4.2.4. Wear under galvanic cathodic protection with Pin On disc

Galvanic cathodic protection using zinc was introduced to suppress corrosion both in sea water and DI water. A cylindrical zinc disc was machined and sanded to make electrical contact with the protected sample. Before experiments, the connectivity between zinc and the sample was tested until good contact was obtained, and then wear experiments were performed. After the experiments, the surface of the samples was observed to see whether corrosion products were formed during the tribocorrosion process.

4.3. Results

4.3.1. Wear rates in different liquids

Figure 4.2 shows the wear rates of samples in three different liquids. As can be seen from Figure 4.2(a), with increasing load, the wear rate increases for all three liquids. In sea water, the wear rate increases almost linearly with load. In ethanol, the wear rate increases linearly for loads up to 5N. For DI water, from 1N to 5N, the wear rate increases slightly, however, at 10N the wear rate is much larger than that at smaller loads. Figure 4.2(b) shows the relation between wear rate and velocity. The wear rate is independent of velocity for DI water and sea water. Only in ethanol, the wear rate slightly increases with increasing velocity. Regardless of velocity, the wear rate in sea water is the smallest among the three liquids, and the wear rate in DI water is

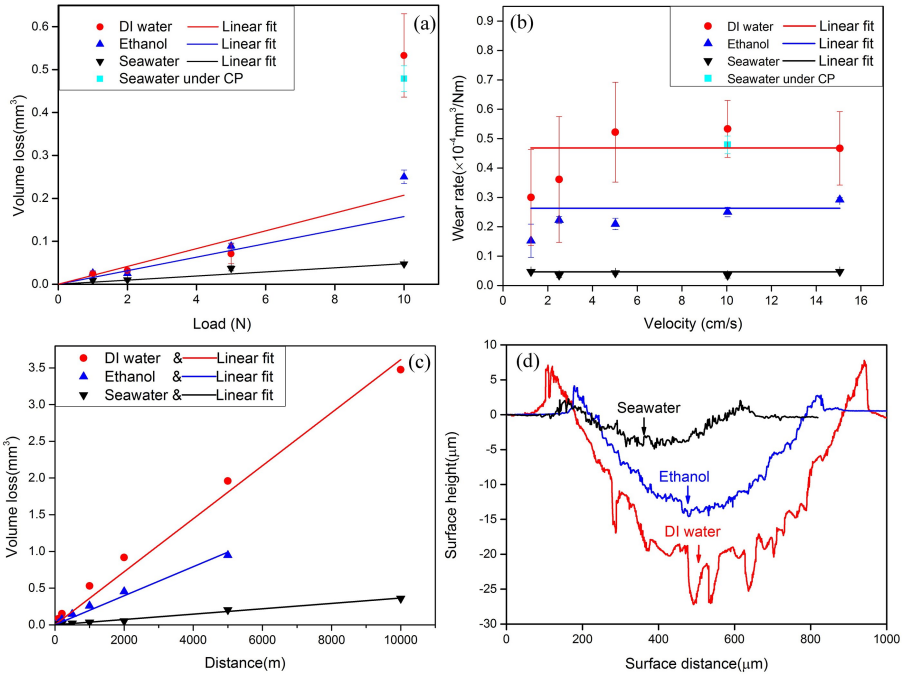

Figure 4.2: Wear rates of the samples in various liquids.(a) Volume loss as a function of load. CP stands for cathodic protection, linear fits were made based on Archard wear equation(from1-5N for ethanol and DI water, from 1-10 N for sea water); (b) Wear rate as a function of velocity, load 10N. (c)Volume loss as a function of distance. Due to the volatile nature of ethanol, 10,000m was not performed. For three liquids, the load and velocity were 10N and 10.04cm/s respectively. (d) Wear tracks of samples in three liquids. load, velocity and distance were 10N, 10.04cm/s and 1,000m respectively

the largest. Figure 4.2(c) shows the relation between wear rate and distance is linear for all three liquids. Clearly, in sea water, the steel wears the least regardless of the load, velocity, and distance. Figure 4.2(d) shows a cross section of the wear tracks in sea water, ethanol and DI water respectively. The wear track of the DI water sample is rather rough compared to another two samples.

4.3.2. Results of immersion experiments in sea water and DI water

Immersion experiments for 24h showed different surface morphology as illustrated in Figure 4.3. For the sample immersed in sea water, white crystals appeared on the surface, and the grain boundaries in the steel can be clearly seen. In contrast, on the surface of the sample immersed in DI water, similar crystals emerged on the surface but no sign of grain boundaries. Some local corrosion appearance was found.

4.3.3. Wear under galvanic cathodic protection with Pin On disc

By applying cathodic protection in sea water, the sample was successfully protected from corrosion with the evidence that the surface was still shiny and no corrosion products were found. The wear rate under this circumstance was higher than that without applying cathodic protection as shown in Figure 4.2(a). However, applying cathodic protection in DI water failed to protect the sample against corrosion. The surface of the sample was rusty and the wear rate did not change at all compared to not applying cathodic protection in DI water.

4.3.4. Friction coefficient comparison and the morphology of the wear track

The friction coefficient is the highest in seawater, the lowest in ethanol, and the intermediate in DI water, as shown in Figure 4.4. No superlubricity occurred in any liquid during the abrasive corrosive wear experiments. Figure 4.5 shows the wear track of the sample worn in sea water. The adjacent area of the wear track shows noticeable protruding phase. The top layer of the ferrite matrix is dissolved. The appearance of protruding phase is not observed in either ethanol or DI water.

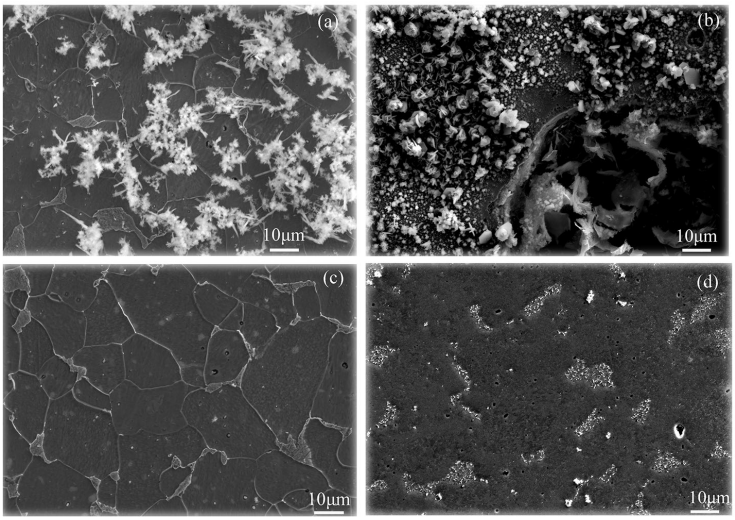

Figure 4.3: Surface morphology after immersed in liquids for 24 hours. (a)surface morphology after immersed in sea water; (b)surface morphology after immersed in DI water; (c) surface of the sample a after removing corrosion products; (d) surface of the sample b after removing corrosion products

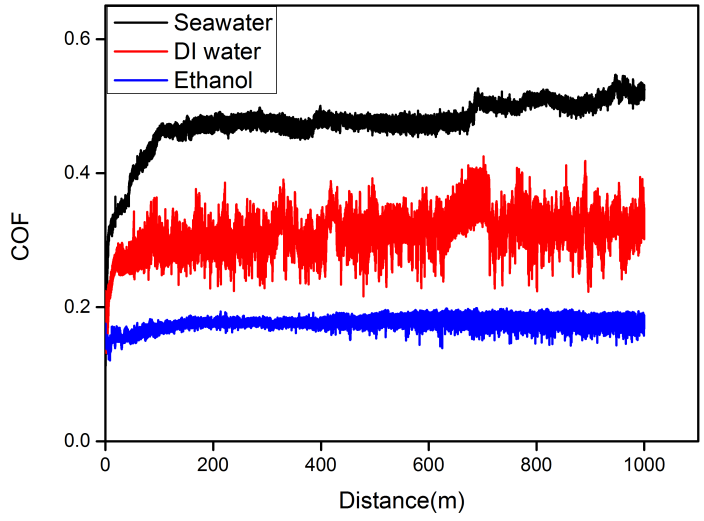

Figure 4.4: Coefficient of friction in various liquids. The load and velocity are 10 N and 10.04 cm/s respectively

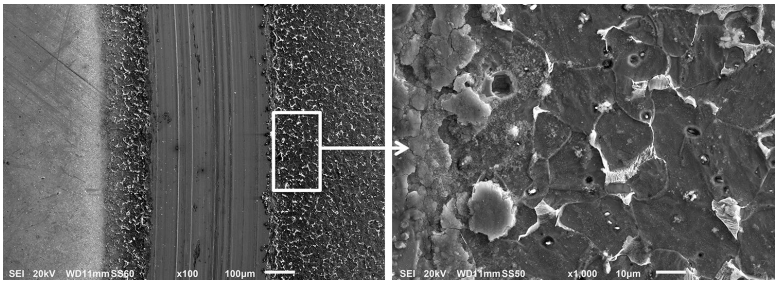

Figure 4.5: The wear track of the sample subjected to wear in sea water. Load and velocity are 10N and 10.04cm/s respectively

4.4. Discussion

Archard in 1953 proposed a model for abrasive wear: volume loss due to wear is proportional to load, sliding distance and inversely proportional to hardness [12]. Wear in ethanol and DI water does not fit this model especially under larger loads, however wear in sea water is in compliance with the model. Moreover, the wear in sea water is less than in ethanol or DI water. During the abrasive corrosive wear process, a surface layer is generated, and that layer diminishes the wear because it is harder than the original material. This explains the lower wear rate of samples in sea water at all velocities as shown in Figure 4.2(b).

Liquids with stronger corrosivity are extensively reported to result in higher wear rate [4–9]. The common explanation attributes this higher wear rate to the rise of chemical wear, the amount of wear caused by the periodic removal of the passive film from the metal surface due to the abrasive action of the counterpart [13–16]. However in the present study, regardless of velocity, wear rates in sea water are all lower than in DI water, while the corrosivity in sea water is higher than that in DI water. Lubrication effects normally have a strong influence in abrasive corrosive wear. However, the COF of samples in sea water is the highest among three liquids as shown in Figure 4.4, the lowest is in ethanol, and DI water is in between, which suggests that the lowest wear rate obtained in sea water is not due to a difference in friction.

The chemical factors, which could lead to surface modification, play a critical role in the abrasive corrosive process.

It has been reported for stainless steel that after the abrasive corrosive wear in sulphuric acid, the surface forms a layer due to corrosion and this layer changes the surface wear resistance [17, 18]. In this study, after immersion test in sea water, grain boundaries were visible, while after immersion in DI water, grain boundaries were not visible as Figure 4.3(c) illustrates. The microstructure of the sample has two constituents, ferrite and pearlite and pearlite consists of ferrite and cementite. When the steel is immersed in sea water, galvanic microcells will be generated between ferrite and cementite due to the electrochemical potential difference [19–21]. The open circuit potential of ferrite is more negative than that of cementite. Therefore the galvanic microcells will lead to the dissolution of ferrite and consequently the protrusion of cementite. Since cementite is harder than ferrite the wear of the steel should be controlled by the cementite in all cases, and hence no difference between sea water, DI water and ethanol would be predicted [22]. The surface in the abrasive corrosive experiment in sea water, enriched in cementite, should become rougher by time, This is however not observed in the wear track in Figure 4.2d.

In this study, the cementite is redistributed over the wear track by the mechanical action of the pin, leading to the observed low wear rate in sea water. The SEM micrograph (Figure 4.5) of the wear track of the sea water sample shows corrosive wear close to the wear track, but hardly any corrosive wear further away from the wear track. Apparently, the abrasive corrosive wear in the wear track leads to corrosive wear close to the wear track. This corrosive wear is also more prominent on the outside of the track than on the inside. The galvanic interaction between the track area and the areas adjacent to the track is responsible for this corrosion. The cementite-covered track will be more noble than the cementite/ferrite areas adjacent to the track leading to enhanced corrosion in those areas. The corroded area outside the track

is at least twice as wide as the area inside the track (Figure 4.5). This difference in width is due to convection in the sea water electrolyte due to the rotation of the disc. When suppressing corrosion in the sea water pin on disc experiment by applying cathodic protection, wear rate increases as shown in Figure 4.2(a) and Figure 4.2(b). This confirms that the surface modification by corrosion plays a critical role in abrasive corrosive wear, leading to elevated abrasive wear resistance in the present study. In DI water due to the non-conductive nature of the liquid, cathodic protection with zinc did not affect the tribocorrosion process therefore the wear rate remained unchanged.

4.5. Conclusions

In this study three liquids were used to research the corrosive abrasive wear behavior of a structural steel S235. In sea water, the wear rate is the lowest because of the surface modification induced by the tribocorrosion process. Cathodic protection was used to verify the influence of corrosion. Increased wear under this circumstance confirms the fact that corrosion increases the wear resistance by modifying the surface of the sample.

References

[1] J. Celis and P. Ponthiaux, *Introduction in" Testing tribocorrosion of passivating materials supporting research and industrial innovation: Handbook",* in *European Federation of Corrosion Series* (Maney Publishing, 2012).

[2] J. Jiang and M. M. Stack, *Modelling sliding wear: From dry to wet environments,* Wear **261**, 954 (2006).

[3] L. Benea, P. Ponthiaux, F. Wenger, J. Galland, D. Hertz, and J. Y. Malo, *Tribocorrosion of stellite 6 in sulphuric acid medium: Electrochemical behaviour and wear,* Wear **256**, 948 (2004).

[4] C. Allen, A. Ball, and B. Protheroe, *The abrasive-corrosive wear of stainless steels,* Wear **74**, 287 (1981).

[5] I. Iwasaki, S. Riemer, J. Orlich, and K. Natarajan, *Corrosive and abrasive wear in ore grinding,* Wear **103**, 253 (1985).

[6] A. Batchelor and G. Stachowiak, *Predicting synergism between corrosion and abrasive wear,* Wear **123**, 281 (1988).

[7] B. Matthes, E. Broszeit, and K. Kloos, *Tribological behaviour and corrosion performance of Ti-B-N hard coatings under plastic manufacturing conditions,* Surface and Coatings Technology **57**, 97 (1993).

[8] S. Watson, F. Friedersdorf, B. Madsen, and S. Cramer, *Methods of measuring wear-corrosion synergism,* Wear **181-183**, 476 (1995).

[9] M. Stemps, S. Mischler, and D. Landolt, *The effect of contact configuration on the tribocorrosion of stainless steel in reciprocating sliding under potentiostatic control,* Corrosion Science **45**, 625 (2003).

[10] European standard EN EN 10025-2:2004, *Hot rolled products of structural steels - Part 2: Technical delivery conditions for non-alloy structural steels,* (2004).

[11] E. Rabinowicz, *Friction and Wear of Materials(2nd edition)* (J. Wiley, 1995).

[12] J. F. Archard, *Contact and rubbing of flat surfaces,* Journal of Applied Physics **24**, 981 (1953).

[13] S. Guadalupe Maldonado, S. Mischler, M. Cantoni, W. J. Chitty, C. Falcand, and D. Hertz, *Mechanical and chemical mechanisms in the tribocorrosion of a Stellite type alloy,* Wear **308**, 213 (2013).

[14] A. C. Vieira, A. R. Ribeiro, L. A. Rocha, and J. P. Celis, *Influence of pH and corrosion inhibitors on the tribocorrosion of titanium in artificial saliva,* Wear **261**, 994 (2006).

[15] Y. Yan, A. Neville, D. Dowson, and S. Williams, *Tribocorrosion in implants-assessing high carbon and low carbon Co-Cr-Mo alloys by in situ electrochemical measurements,* Tribology International **39**, 1509 (2006).

[16] P. Jemmely, S. Mischler, and D. Landolt, *Electrochemical modeling of passivation phenomena in tribocorrosion,* Wear **237**, 63 (2000).

[17] J. Perret, E. Boehm-Courjault, M. Cantoni, S. Mischler, A. Beaudouin, W. Chitty, and J. P. Vernot, *EBSD, SEM and FIB characterisation of subsurface deformation during tribocorrosion of stainless steel in sulphuric acid,* Wear **269**, 383 (2010).

[18] N. Diomidis, J. P. Celis, P. Ponthiaux, and F. Wenger, *Tribocorrosion of stainless steel in sulfuric acid: Identification of corrosion-wear components and effect of contact area,* Wear **269**, 93 (2010).

[19] G. Kehl, *The principles of metallographic laboratory practice*, 3rd ed. (Mcgraw-Hill Book Company, New york, 1949).

[20] R. Nyborg, E. Gulbrandsen, T. Loeland, and K. Nisancioglu, *Effect of Steel Microstructure and Composition on Inhibition of CO_2 Corro-*

sion, in *Corrosion 2000* (NACE International, Orlando, Florida, 2000) pp. NACE–00023.

[21] H. Zhang, S. Ohsaki, S. Mitao, M. Ohnuma, and K. Hono, *Microstructural investigation of white etching layer on pearlite steel rail,* Materials Science and Engineering: A **421**, 191 (2006).

[22] B. Bhushan, *Principles and Applications of Tribology, Second Edition* (John Wiley and Sons, 2013).

5

Impacting wear of structural steel with a yield strength of 235 MPa in various liquids

The first principle is that your must not fool yourself
and you are the easiest person to fool

Richard Feynman

This chapter is based on the following article:
Yueting Liu, G.C.A.M. Janssen, Impacting wear of structural steel with a yield strength of 235 MPa in various liquids (submitted to Coatings)

5

This chapter presents the impacting wear of structural steel. The wear mechanism involves abrasion, corrosion, impacting, and the interaction among them. The impacting effect on the wear mechanism and wear rate was investigated. Results show that when impacting effect is small, the wear mechanism is dominated by electrochemically induced surface modification, which leads to lower wear rate in corrosive environment than in non-corrosive environment. By contrast, when impacting effect is large, the wear mechanism is drastically altered. In that regime plastic deformation is important. The influence of corrosion in the high impacting regime is negligible. The findings show the importance to distinguish between abrasive- and impacting-wear in corrosive and non-corrosive environments.

5.1. Introduction

Dredging is involved to keep waterways navigable or to construct new land in freshwater or seawater areas. In dredging engineering, the sedimented sands or other solids, mixed with water, need to be transported using pipelines. The pipelines wear due to the interaction between abrasive wear and corrosion, resulting in high costs for maintenance and replacement of the pipelines [1–3].

Researchers have studied and reported the wear of pipelines for decades [4–10]. Truscott reviewed the research of 20 years before 1972 and summarized three determinant factors of wear: the properties of the slurry, the regime of the flow and the materials [11]. The properties of slurry mainly include the particle hardness, size, shape (sharpness), specific mass, concentration. The mode of flow in principle determines the particle dispersion and particle motion, which eventually influences the wear mechanism. The properties of materials mainly include chemical composition, microstructure and hardness. The wear of slurry pipelines results mainly from two mechanisms, particle impacting and scouring, where the latter occurs as a result of a sliding abrasive wear. Several apparatuses have been introduced to study the wear mechanism of slurry pipes [12, 13]. These apparatuses aim to study the influence of multiple factors like the flow concentration, the particle size, or the flow velocity.

However, the material surface change due to corrosion is rarely reported, yet extremely important. In a corrosive environment, especially in electrochemical corrosion, the surface of the material changes and the change could potentially alter the original material properties like hardness, and therefore it influences the final wear rate. In chapter 4, the micro-coupling effect is reported to be able to decrease the wear rate, with a multi-phase material in an electrochemically corrosive environment [14]. In that study, a structural steel, containing ferrite and cementite, was exposed in sea water while

subject to abrasive wear. The coupling between ferrite and cementite, due to their electrochemical potential difference, leads to the dissolution of ferrite and the protruding of cementite, and subsequently the redistribution of cementite due to abrasion. The altered surface is much harder than the original due to the enrichment of harder phase: cementite.

In actual slurry transport, however, no noticeable wear rate decrease in sea water was observed and reported. In this study, impacting is introduced to identify the wear mechanism. Various liquids are used to provide various corrosive environments. Impacting effect is found to dominate in this study. The domination of impacting wear explains the negligible difference in wear in sea water and fresh water.

5.2. Experimental

5.2.1. Material preparation

The material, used in this study, is a structural steel: S235 [15]. This material, with a minimum yield strength of 235 MPa, is widely used in dredging industry for its good combination of mechanical properties and welding properties. The sample used in this study are cylinders, 30 mm in diameter and around 8 mm in thickness. The preparation procedure consists of three stages. First, the sample was sanded with silicon carbide sandpaper from 80 mesh to 2400 mesh (particle size equals roughly 10 μm). Then the sanded sample was polished with diamond containing polishing liquids, until the surface of the sample was mirror-like. The size of the diamond in the polishing liquids was from 3 μm to 1 μm. Finally, the polished sample was cleaned in acetone with ultrasonic, followed by rinsing with distilled water and dried with room temperature air. The counterpart used in this study was an aluminum oxide ball with a diameter of 6 mm. After each experiment, the ball was either rotated or replaced to obtain fresh contact between the sample and the ball.

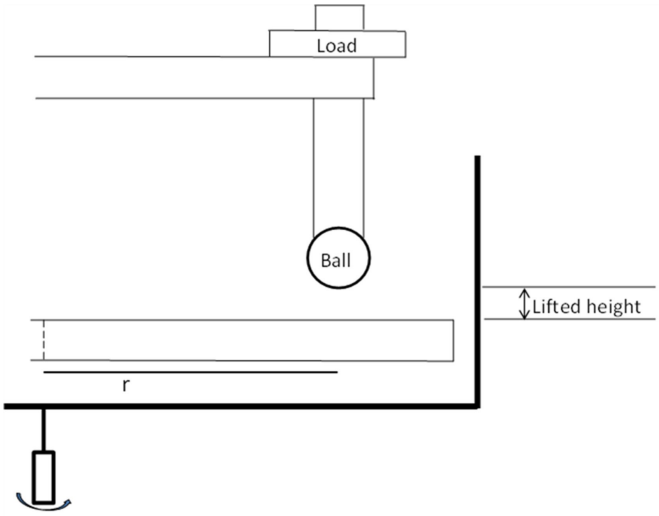

Figure 5.1: The diagram of the modified pin on disc. A lifted distance exists between tha ball and the sample surface. The distance is well controlled and measured the software of pin on disc.

5.2.2. Experimental procedure with a hammering pin on disc

A modified pin on disc, as shown in Figure 5.1, was used to perform experiments. A hammering module was incorporated. The module contains a retractable component, powered by compressed air and controlled by a LabView program, to hit and lift the pin. The lifted height can be measured during experiments by the pin on disc software. The load was 1 N for all experiments but with various lifted height, thereby various impacting effect, namely 0.2 mm, 1.0 mm, 2.0 mm, 3.3 mm. The pin was lifted at a frequency of 1Hz and in contact with the sample for a period close to 0.5s. The pin hit the sample at a near but different place each time, forming a round wear track eventually. The radius was 8 mm, and the rotational speed was 2Hz for each 2.75-hour experiment. Three liquids were used to provide different corrosion condition, namely non-corrosive ethanol, corrosive deionized water, and severely corrosive sea water (simulated by a 3.5% NaCl solution). Each combination of lifted height and liquid was repeated three times to

obtain the variability of the experiment.

5.2.3. Characterization

After experiments, the wear track profiles of the samples were measured by white light interferometry. Specifically, four different places of each cross section of the wear track were measured, and the wear rate was calculated by multiplying the area of the cross section by the perimeter of the wear track, divided by the sliding distance [16].

5.3. Results

5.3.1. Wear rate comparison for various lifted height

Wear rate, overall, increased with increasing lifted height from 0.2 mm to 3.3 mm, as shown in Figure 5.2a. For the case of 0.2 mm, the wear rate in deionized water was the largest, followed by wear in ethanol. In sea water, the wear rate was the smallest. This order is the same as was obtained in sliding wear in these liquids [14]. For higher lifted heights, the wear rate difference among three liquids decreases. At 1.0 mm lifted height, the wear rate in the three liquids is identical within the error of measurement. For higher lifted heights the differences are even smaller. The net material loss, shown in Figure 5.2b, shows the same behavior, except that the wear rate increase with the increasing lifted height is much smaller.

5.3.2. Wear track analysis

The wear track comparison at various lifted height in three liquids is illustrated in Figure 5.3. As can be seen, for each liquid, with increasing lifted height, the depth of the track increases as well, and when the lifted height reaches 3.3 mm, the wear depth seems to be the same among all liquids, well corresponding to the wear rate comparison (Figure 5.2). The total

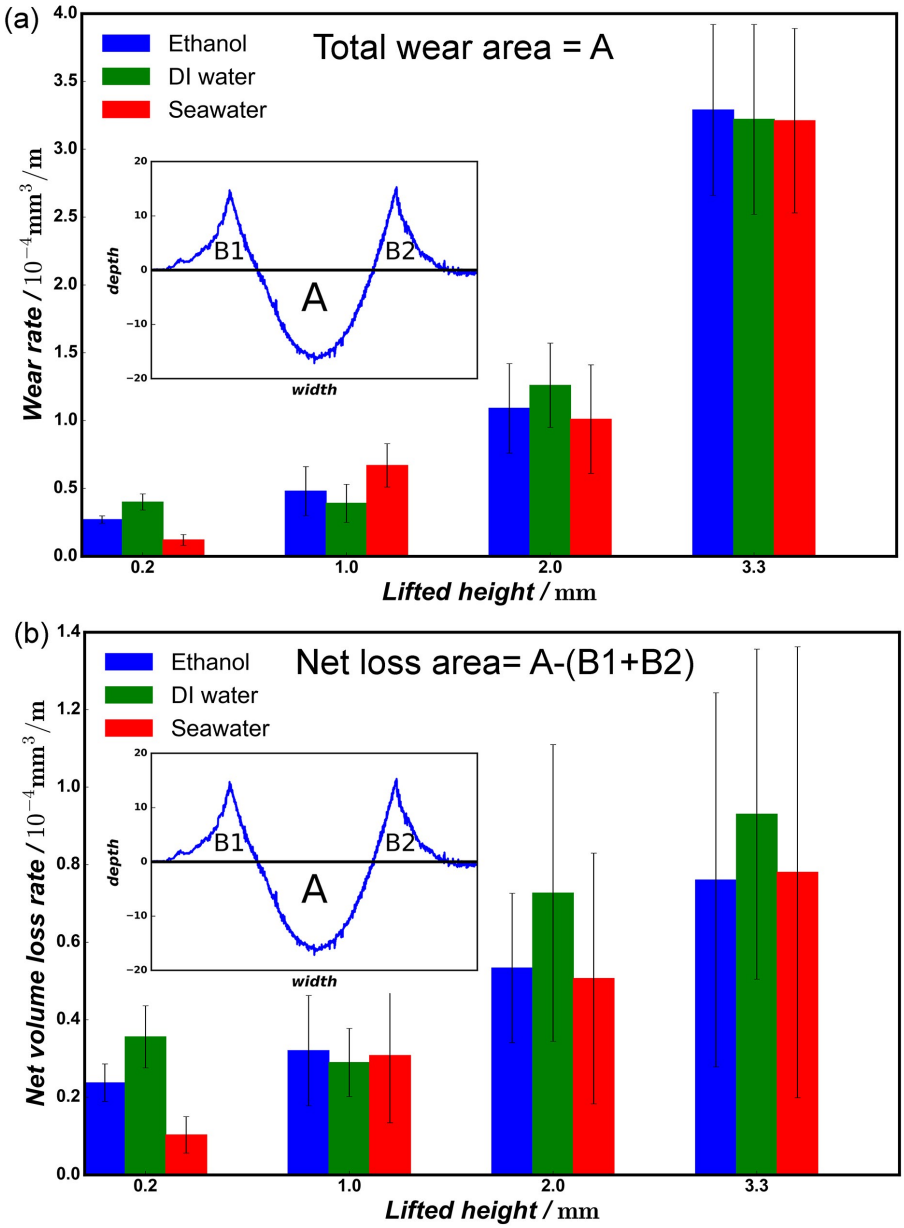

Figure 5.2: (a) Wear rate comparison at various lifted height; (b) Net volume loss comparison at various lifted height. Ethanol, DI water and sea water were used to vary corrosivity. The error bar stands for one standard deviation of three repeated results. The embedded small figure represents the cross section of the round wear track.

volume loss due to wear has two components: material removal and deformation. The deformation part accounts for a large portion of the total wear when the lifted height is beyond 1 mm. As shown in Figure 5.4, for all three liquids, the ratio of deformation to total wear is less than 20% for the lifted height of 0.2 mm, by comparison, it reaches almost 80% when the lifted height is 3.3 mm. For 1.0 mm and 2.0 mm, the ratios are comparable. In sea water, the ratio change is the most dramatic from less than 20% to roughly 60%, when the lifted height increases from 0.2 mm to 1.0 mm. Additionally, the wear track, overall, is smooth except for the situation where the lifted height is the least, 0.2 mm, which shows a level of roughness, similar to the situation in pure sliding [14].

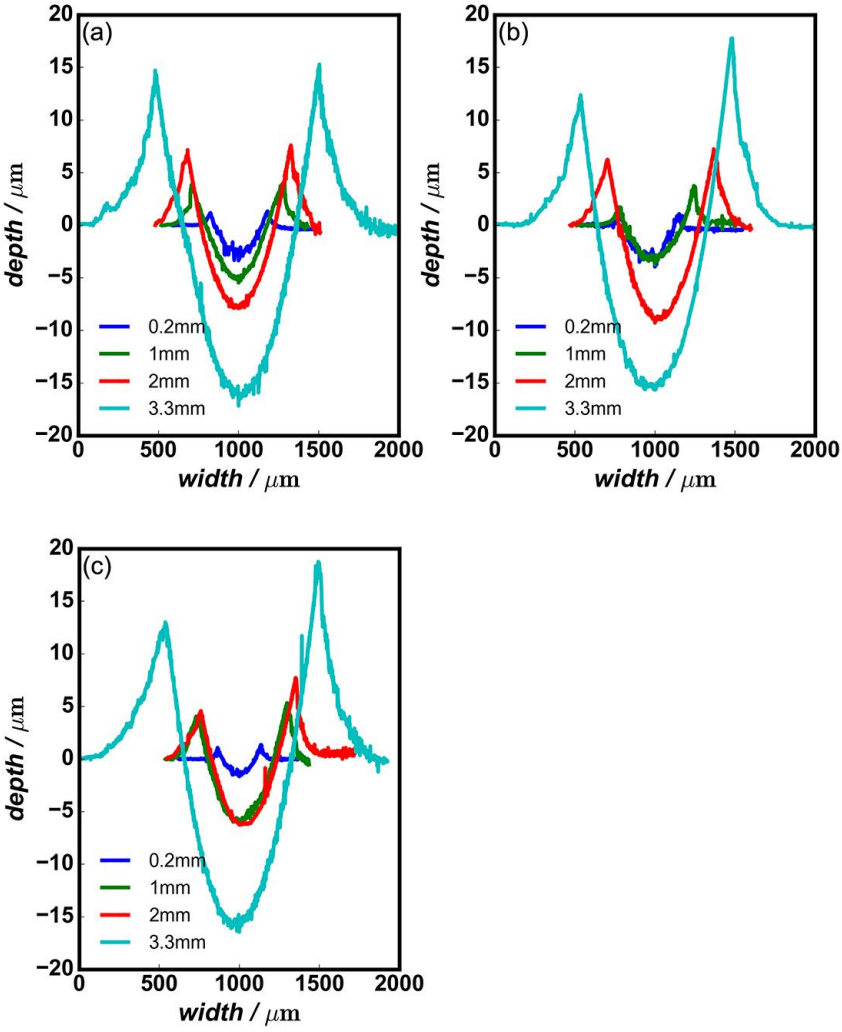

Figure 5.3: Wear track comparison at various lifted height in three liquids. (a) in ethanol; (b) in DI water; (c) in sea water. The average of three repetitive results was used for each situation. The wear track was moved to the center in order to be easily compared.

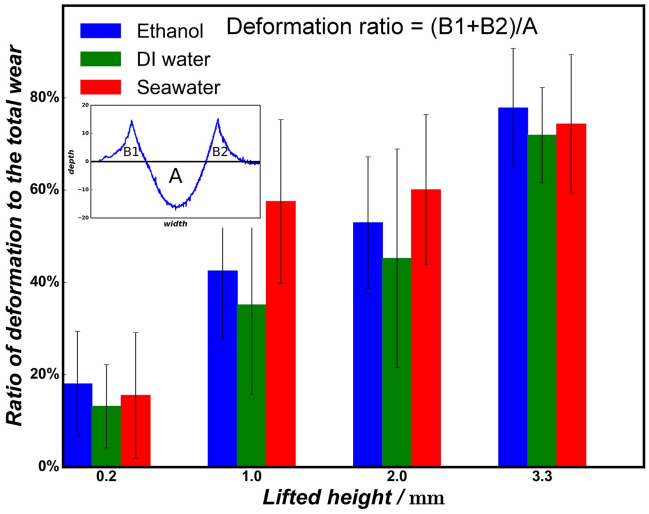

Figure 5.4: The ratio of deformation to total wear at various lifted height. Ethanol, DI water and sea water were used to vary corrosivity. The error bar stands for one standard deviation of three repeated results. The embedded small figure represents the cross section of the round wear track.

5.4. Discussion

In slurry transport, the pipes wear due to the combination of sliding, impacting and corrosion [1]. The interaction among those factors determines the final wear. Typically, the interaction leads to a positive synergistic effect and results in higher wear rate. However, research has shown the beneficial effect of the interaction between corrosion and abrasion, where corrosion can modify the sample surface by dissolving the soft phase and leaving the hard phase protruding, and subsequently, abrasion redistributes the hard phase, increasing the wear resistance [14]. However, in real slurry transport situations, no noticeable wear difference between corrosive and non-corrosive mediums was observed and reported. Although the scale of the research in a lab is different from in real situation, the mechanisms should be the same. In this study, impacting shows a huge influence on the wear rate. At 0.2 mm, the wear rate in ethanol, DI water, and sea water is very different, and

in sea water, the wear rate is the smallest. However, when the lifted height is increased to 1.0 mm, the wear rate difference is within the experimental uncertainty. From 1.0 mm lifted height upwards, the influence of corrosion is not able to dominate. At 0.2 mm, the impacting is small, and the wear result is similar to the result found in pure sliding. In pure sliding, the modified surface can increase the wear resistance of the sample, showing a beneficial effect. From low impact to high impact, the wear mechanism changes from material removal to mainly deformation, as shown in Figure 5.4. When deformation becomes the main factor of wear, surface modification, which governs the wear mechanism in pure sliding, does not make a difference. The deformation also results in a rather smooth wear track, which is not typical in a corrosive environment. The smooth wear track implies that the influence of corrosion becomes less important.

5.5. Conclusions

In this study, the effect of impacting on the wear of a structural steel S235 was studied in various liquids. When impacting is small, corrosion plays a dominant role so that the sample in sea water wears the least due to the beneficial interaction with abrasion. However, when impacting is large, the wear rates among three liquids do not show noticeable difference, because of the wear mechanism change from material removal to mainly deformation. The influence of corrosion is not dominant in the case of impacting wear.

References

[1] K. C. Wilson, G. R. Addie, A. Sellgren, and R. Clift, *Slurry Transport Using Centrifugal Pumps* (Springer, 2006).

[2] M. C. Roco and G. R. Addie, *Erosion wear in slurry pumps and pipes,* Powder Technology **50**, 35 (1987).

[3] M. Jones and R. J. Llewellyn, *Erosion-corrosion assessment of materials for use in the resources industry,* Wear **267**, 2003 (2009).

[4] R. C. Shivamurthy, M. Kamaraj, R. Nagarajan, S. M. Shariff, and G. Padmanabham, *Influence of microstructure on slurry erosive wear characteristics of laser surface alloyed 13Cr-4Ni steel,* Wear **267**, 204 (2009).

[5] C. S. Ramesh, R. Keshavamurthy, B. H. Channabasappa, and S. Pramod, *Influence of heat treatment on slurry erosive wear resistance of Al6061 alloy,* Materials and Design **30**, 3713 (2009).

[6] S. Bross and G. Addie, *Prediction of impeller nose wear behaviour in centrifugal slurry pumps,* Experimental Thermal and Fluid Science **26**, 841 (2002).

[7] N. M. Dube, A. Dube, D. H. Veeregowda, and S. B. Iyer, *Experimental technique to analyse the slurry erosion wear due to turbulence,* Wear **267**, 259 (2009).

[8] G. B. Tupper, I. Govender, A. N. Mainza, and N. Plint, *A mechanistic model for slurry transport in tumbling mills,* Minerals Engineering **43-44**, 102 (2013).

[9] N. Ojala, K. Valtonen, A. Antikainen, A. Kemppainen, J. Minkkinen, O. Oja, and V.-T. Kuokkala, *Wear performance of quenched wear resistant steels in abrasive slurry erosion,* Wear **354-355**, 21 (2016).

[10] S. S. Rajahram, T. J. Harvey, and R. J. K. Wood, *Erosion-corrosion resistance of engineering materials in various test conditions,* Wear **267**, 244 (2009).

[11] G. F. Truscott, *A literature survey on abrasive wear in hydraulic machinery,* Wear **20**, 29 (1972).

[12] T. Deng, M. S. Bingley, M. S. A. Bradley, and S. R. De Silva, *A comparison of the gas-blast and centrifugal-accelerator erosion testers: The influence of particle dynamics,* Wear **265**, 945 (2008).

[13] J. J. Tuzson, *Laboratory slurry erosion tests and pump wear rate calculations,* Journal of Fluids Engineering **106**, 135 (1984).

[14] Y. Liu, J. M. C. Mol, and G. C. A. M. Janssen, *Corrosion reduces wet abrasive wear of structural steel,* Scripta Materialia **107**, 92 (2015).

[15] European standard EN EN 10025-2:2004, *Hot rolled products of structural steels - Part 2: Technical delivery conditions for non-alloy structural steels,* (2004).

[16] E. Rabinowicz, *Friction and Wear of Materials(2nd edition)* (J. Wiley, 1995).

6

Conclusions and Future work

Life is 10% what happens to you and 90% how you react to it

Charles Swindoll

Conclusions:

This dissertation focuses on the interaction between corrosion and mechanical wear, especially in the case of slurry transport. A better understanding of the combined wear mechanism is the key to selecting or developing suitable materials. Below, first the conclusions from the individual chapters are reviewed. Subsequently the results are combined and treated in relation to the "state of the art"at the beginning of my PhD research.

The popular model of the cyclic formation and removal of corrosion film in abrasive-corrosive wear was indeed observed in aluminum alloy 7075-T6 as presented in chapter 2. Additionally, imposing a cathodic potential was not able to fully suppress corrosion, as intergranular or pitting corrosion were still observed and they contribute to the final wear rate as well. The combined wear mechanism is that the increase of the uniform corrosion results in an increase of wear rate due to the cyclic formation and removal of the corrosion film. Moreover, in the case of cathodic protection, the wear rate does not drop noticeably but remain comparable with the wear rate at the open circuit potential, due to the occurrence of intergranular or pitting corrosion.

The slurry loop study, as presented in chapter 3, does not show that the wear rate of steel in seawater is smaller or larger than the wear rate in fresh water. Additionally, the sample alignment and size are critical to performing experiments in slurry loop. The wear rate, in chapter 3, is represented by the surface roughness after wear experiments. Since the sample was polished until mirror-like, the surface roughness was zero (negligible) before experiments. The surface roughness after experiments can be fully attributed to the wear of the sample. The roughness comparison does not show a noticeable difference of wear rate in seawater and freshwater. However, the roughness does show non-uniformity in both liquids, indicating the alignment and size of the sample are critical.

The interaction between corrosion and abrasive wear was long reported to

increase the wear rate, but for structural steel with a minimum yield strength of 235 MPa (S235), the results show just the opposite as presented in chapter 4. The main finding here is that for S235 in a corrosive and conductive environment, phases with different electrochemical potentials can couple together to form a galvanic micro-cell. In the micro-cell, one phase is dissolved, the other is left. As presented in chapter 4, in the micro-cell formed between ferrite and cementite, ferrite is dissolved first due to its relative more active electrochemical property, leading to the protruding of cementite. The protruded cementite is then redistributed due to abrasive wear and that leads to a modified surface layer enriched in cementite, which is much harder than ferrite. The wear resistance was enhanced instead of reduced. Moreover, when the sample was subject to cathodic protection to suppress corrosion, the wear rate increased, confirming that corrosion is beneficial and can enhance wear resistance.

However, the modified surface layer is not necessarily able to enhance wear resistance when impacting is involved, as the layer may not survive the impacting. Chapter 5 presents the findings that the wear rate difference in various corrosive environments disappears when impacting effect is significant. The surface modification, cannot sustain high impacting wear.

Before the start of my PhD research, it was believed that corrosion always accelerates wear. A TNO study, conducted by Mens and de Gee, studies wear in a slurry pot filled with sand and seawater. The materials studied are carbon steels and high chromium cast irons [1]. The key figure form their publication is reproduced in figure 6.1.

Their results, illustrated in figure 6.1, show that for carbon steels, the wear resistance scales linearly with hardness. The high chromium cast irons have a much higher wear resistance. The high chromium cast irons have a hardness between 700 and 850 HV. The blue diamond data points at around (800, 6) are samples composed of 2-3% of carbon and 14-18% of chromium. By comparison, the blue diamond data point at (680, 12) is the sample with

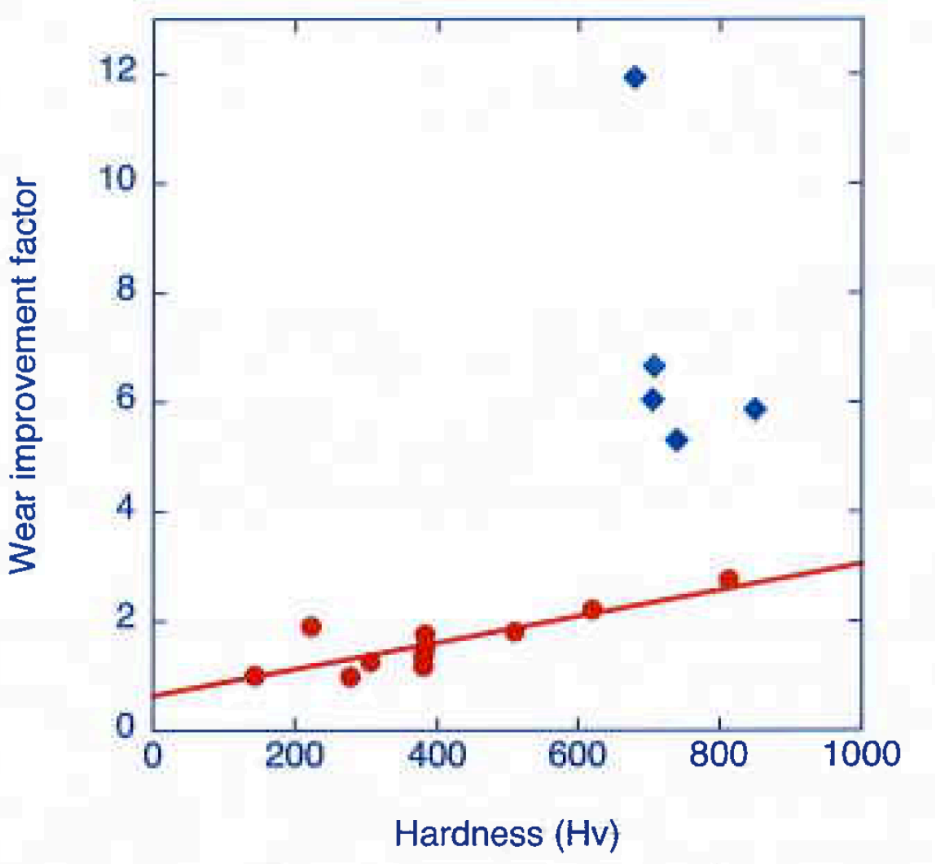

Figure 6.1: Wear improvement factor for various alloys, as function of hardness. The red dots represent carbon steels, and the blue diamonds represent high chromium cast irons [1].

25% of chromium (the highest chromium content of all the samples). The wear resistance of the high chromium content cast irons is roughly proportional to the chromium content. In the proposal for my PhD project it was speculated that this was because more chromium means less corrosion and since corrosion increases wear rate, a material that has high corrosion resistance has high wear resistance as well. Now, with the findings presented in this thesis, it is clear that the influence of corrosion on wear is complex. Corrosion may accelerate wear rate as in the case of cyclic formation and removal of surface corrosion products, presented in chapter 2. Also, corrosion may decrease wear rate as in the case of galvanic micro-coupling, presented in chapter 4. Additionally, corrosion may not influence wear rate as in the case of high impacting wear, as presented in chapter 5. To summarize, the influence of corrosion on wear is highly determined by the specific situation. To go back to the results of the TNO study of Mens and de Gee, the high wear resistance of high chromium cast iron is most likely not due to the high corrosion resistance, but to the microstructure, specifically to hard chromium carbides embedded in soft and ductile matrix. The hardness of the chromium carbide precipitates is estimated to be around 1800 HV micro hardness [2–4]. The combination of hard-phase particles and ductile matrix has been reported to lead to high strength and high toughness. In high chromium cast irons, chromium carbides combined with the matrix, have been reported to be the main reason of their high wear resistance [2]. In a study, researchers conclude that the best combination is a ductile matrix and chromium-rich carbides (with up to 1800 HV micro hardness). A specific type of carbides, M7C3, are able to provide a barrier against indentation, grooving and cutting. These studies suggest that the main reason responsible for the high wear resistance of high chromium cast irons in a corrosive slurry pot experiment is not their corrosion resistance as hypothesized before, but their unique microstructure.

Overall, the influence of corrosion on wear is found to be much more complex

than proposed at the onset of my PhD research. The new findings in this thesis show that the influence of corrosion is highly dependent on the specific situation and the corresponding wear mechanism. Corrosion may increase wear rate when the process is governed by cyclic formation and removal of surface corrosion products. Corrosion may decrease wear rate when the process is governed by galvanic micro coupling effect. Corrosion may not influence wear rate when the process is dominated by impacting.

Future work:

Understanding the interaction between wear and corrosion is critical to a deeper understanding of the degradation of materials. In chapter 3 and 4, two different mechanisms were presented for corrosive abrasive wear. In case it is desired to have a high wear resistance in the case of corrosive-abrasive wear one is directed to steels with a microstructure that under corrosive conditions may yield a carbon rich top layer that is resistant to corrosive abrasive wear.

In chapter 5 it is shown that for slurry transport one should consider impacting-corrosive wear instead of abrasive-corrosive wear. For slurry transport applications, I see two directions:

1. Steels or cast irons with hard precipitates, like the materials studied by Mens and de Gee.
2. Impacting resistant steels.

Impacting resistant steels have high toughness. If high toughness is combined with high hardness and ductility, the steel is very likely to exhibit high wear resistance under high impacting wear. A candidate for further research into preventing impacting wear is Hadfield steel. Hadfield steel contains unstable austenite at room temperature due to the large amount of austenite stabilizer: Manganese (11-15%). The austenite is ductile and

it will transform to martensite when subject to mechanical impact, forming a hard surface layer.

References

[1] J. W. M. Mens and A. W. J. de Gee, *Erosion in seawater sand slurries,* Tribology International **19**, 59 (1986).

[2] M. Buchely, J. Gutierrez, L. Leon, and A. Toro, *The effect of microstructure on abrasive wear of hardfacing alloys,* Wear **259**, 52 (2005).

[3] Y. Li, Y. Gao, B. Xiao, T. Min, Y. Yang, S. Ma, and D. Yi, *The electronic, mechanical properties and theoretical hardness of chromium carbides by first-principles calculations,* Journal of Alloys and Compounds **509**, 5242 (2011).

[4] R. Gundlach and J. Parks, *Influence of abrasive hardness on the wear resistance of high chromium irons,* Wear **46**, 97 (1978).

A

Supplementary materials of tribocorrosion of aluminum alloy 7075-T6

A

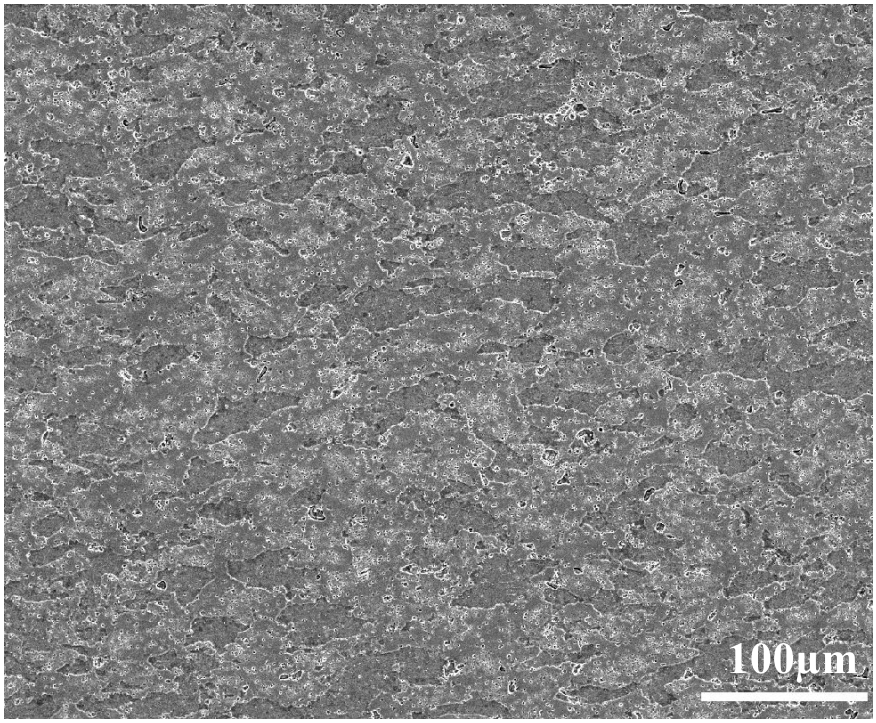

Figure A.1: Top view micrograph of the AA7075-T6 base substrate. Keller's reagent was used to etch the sample.

Table A.1: Chemical composition of the AA7075-T6 base substrate. The composition was measured with XRF. The measurements were performed with a Panalytical Axios Max WD-XRF spectrometer and data evaluation was done with SuperQ5.0i/Omnian software

Element	Al	Zn	Mg	Cu	Cr	Fe	Si
Content(wt%)	89.665	5.365	2.55	1.719	0.244	0.184	0.115
Absolute error(%)		0.07	0.05	0.04	0.01	0.01	0.01
Element	Ga	Mn	Ti	Cl	V	Zr	Ni
Content(wt%)	0.046	0.043	0.031	0.021	0.009	0.006	0.004
Absolute error(%)	0.006	0.006	0.005	0.004	0.003	0.002	0.002

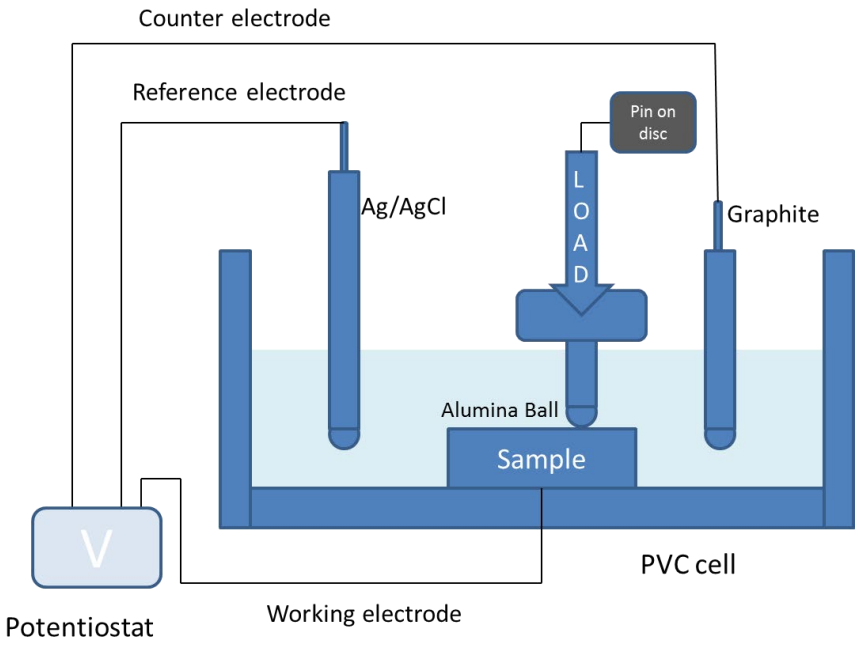

Figure A.2: Schematic representation of the tribocorrosion setup. An Autolab potentiostat was used to perform potentiostatic experiments and to record corrosion current response data.

A

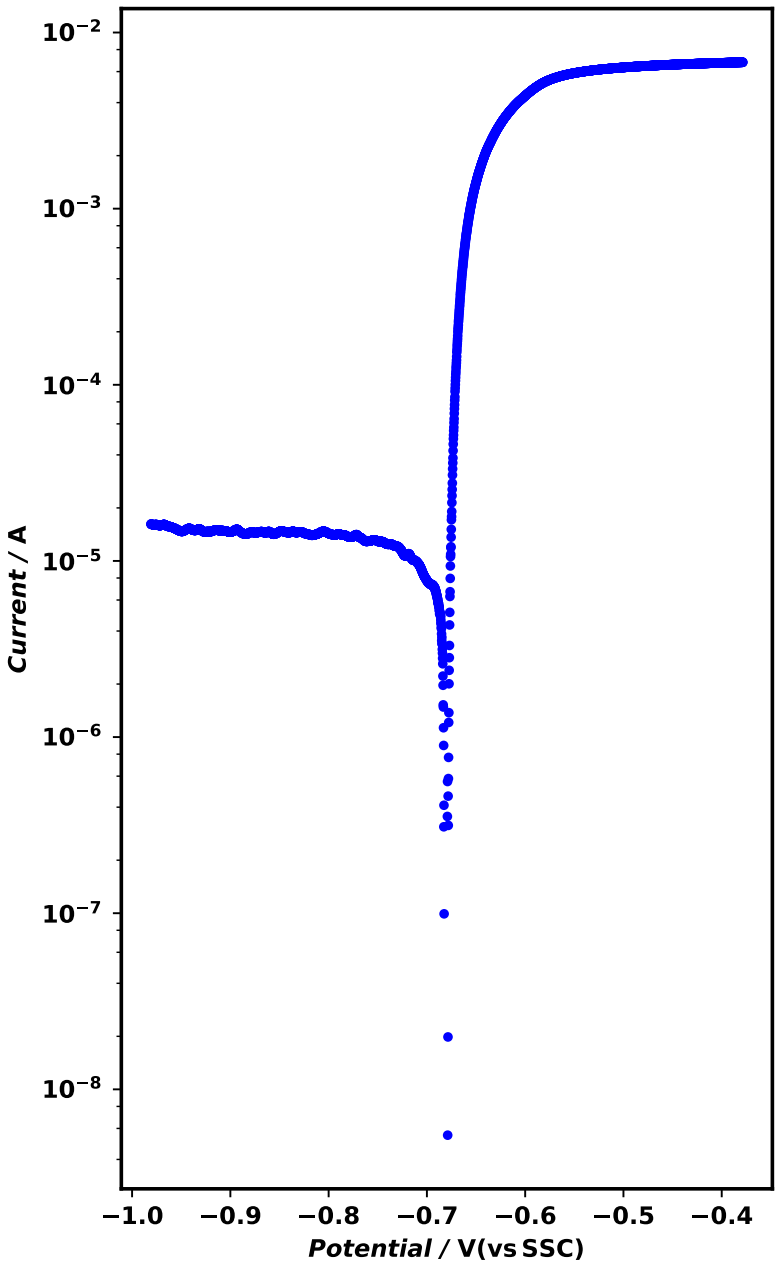

Figure A.3: Polarization curve of AA7075-T6 in 3.5% NaCl solution. All applied potentials are relative to standard silver/silver chloride electrode. The OCP is measured as -0.68 V. The measurement starts after the sample surface reaches a stable state at OCP.

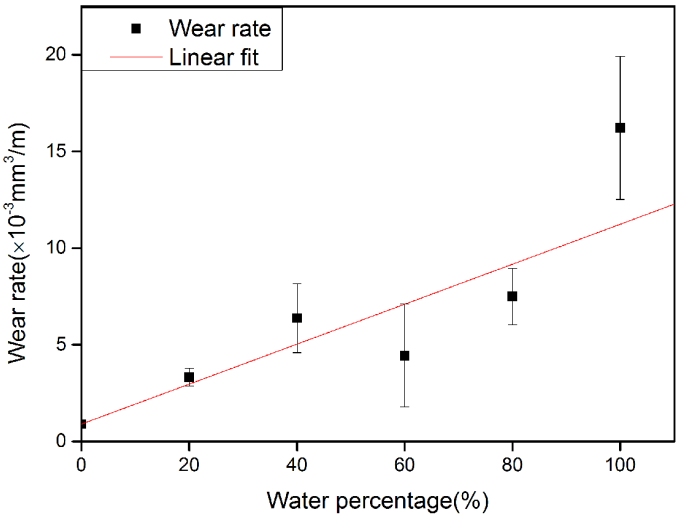

Figure A.4: Wear rate as a function of water percentage. The wear rate increases with increasing water percentage, indicating that corrosion enhances wear in the ethanol-water system. This result keeps in agreement with other two series of experiments presented in chapter 2. The two series of experiments were performed in various liquids and various imposed electrochemical potentials. Both sets facilitate variation of corrosivity in order to study the wear change respect to the corrosion change (credit to the bachelor final project 'Natte slijtage van aluminium 7075T6')

B

Supplementary materials for slurry loop experiments

Table B.1: particle size, concentration and the medium of the slurry that used in the experiments of chapter 3. Two particles size were used, as well as two concentrations and two mediums.

Sand type	Concentration	Medium
Dorsilit 8 (0.3-0.8 mm)	10%, 20%	Salt water, fresh water
Dorsilit 7 (0.6-1.2 mm)	10%, 20%	Salt water, fresh water

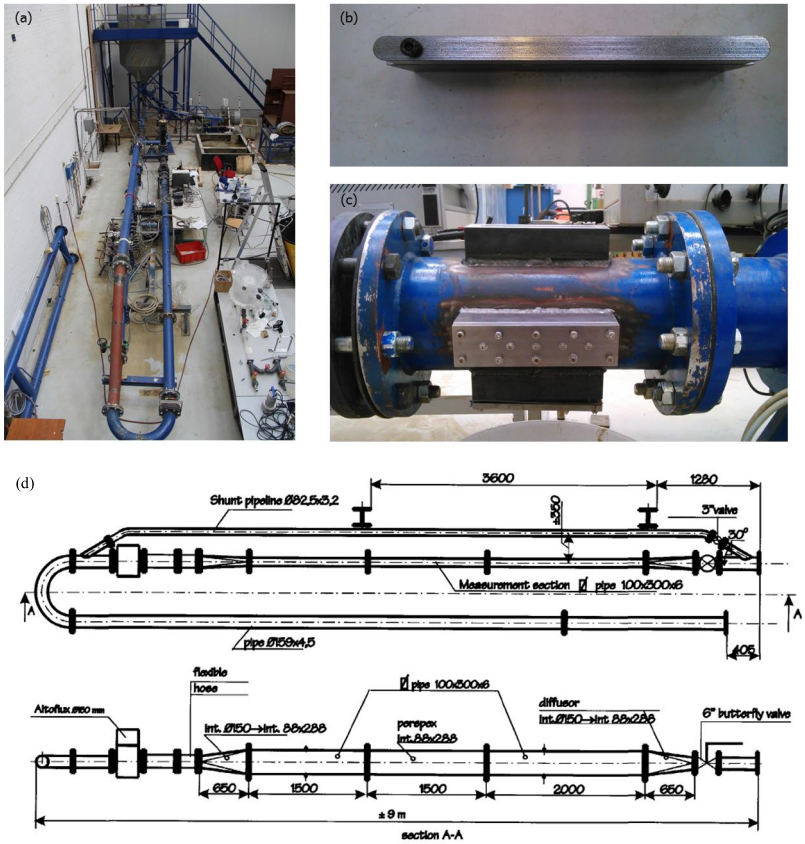

Figure B.1: Slurry loop setup, the sample and the sample positioning. (a) The slurry loop setup; (b) The sample with a screw on the left to seal an area as the reference point during measurement; (c) The position of the sample in slurry loop, including top, side and bottom. (d) Modified test section by van Rhee. The slurry loop setup used in this study was different from the original slurry test circuit as shown in Figure 3.1, but with modifications.

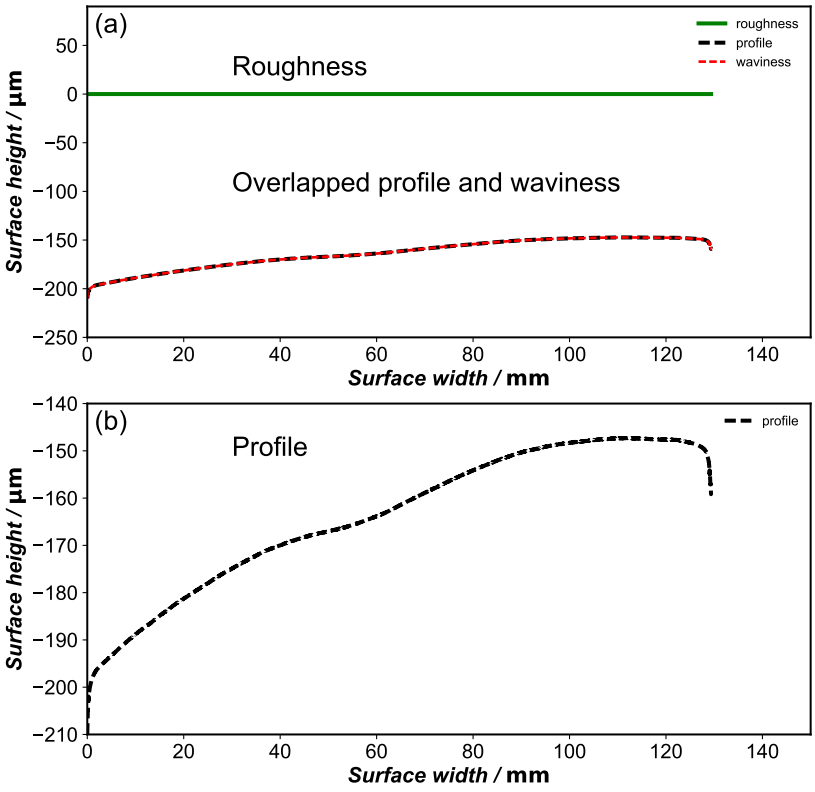

Figure B.2: Roughness of the sample before experiments. (a) shows the roughness, primary profile, and waviness; (b) shows the primary profile. Note the scale difference between (a) and (b). The initial surface is curved, as shown in (b), but with the cut-off, used in the data processing, the curvature is categorized as waviness, and therefore the initial roughness is negligible (zero), as shown in (a), the primary profile and waviness overlap with each other.

Summary

Dredging is an important industry. A key component of dredging is slurry transport. The main problem of slurry transport is the wear of the used piping. This thesis is concerned with the materials science aspects of the wear of the pipelines used in slurry transport.

A better understanding of the wear mechanism of materials is essential to selecting suitable materials to prolong service time and reduce costs. Wear resistance is not an intrinsic material property but a response to a system including multiples parameters determined by the material, the counter body, the load condition, and the environment. In the particular environment of slurry transport, wear is coupled with corrosion, a well-known cause of materials degradation. When mechanical wear and corrosion co-exist, they interact with each other and, often, enhance each other, resulting in faster material failure than the situation where only a single factor exists. This thesis presents the study of the interaction between corrosion and wear with the goal of obtaining a better understanding of the wear mechanism to guide the material selection. To study the wear mechanism, a pin on disc tribometer was employed to precisely control the load, rotational speed, and corrosion environment. A potentiostat was also used to provide well-defined corrosion environment (corrosion is quantified by the current and potential). By connecting the pin on disc with a potentiostat, a well-controlled mechanical and chemical (electrochemical) system was employed to perform wear experiments.

Chapter 1 introduces the field where the problem originates and identifies the problems to be solved. A general introduction to the problem of wear

and corrosion is presented, followed by a short summary of the research in the field. Finally, the common techniques used to study the interaction between mechanical wear and corrosion are summarized.

In chapter 2, it is shown that the cyclic formation and removal of corrosion products is the main wear mechanism of aluminum alloy 7075-T6 in a corrosive and abrasive environment. In two series of measurements, namely in various liquids and in various imposed potentials to vary the corrosion conditions, the wear rate in sea water is higher than that in deionized water and ethanol; The wear rate subjected to an anodic potential is higher than the wear rate subjected to the open circuit potential or a cathodic potential. Additionally, when the imposed potential is in the anodic area, the wear rate increases with increasing potential. These findings demonstrate the enhancing effect of corrosion on wear. Additionally, of the three liquids, the wear rate in non-corrosive ethanol is distinctly smaller (over a factor of 20) than that in sea water. However, in the potentiostat series, the wear rate of the sample when subjected to the cathodic potentials (in order to invoke cathodic protection) does not drop sharply, compared to the condition at the open circuit potential. The reason is that cathodic protection is only able to suppress uniform corrosion, but not intergranular corrosion caused by strengthening precipitation particles, or localized corrosion caused by intermetallics.

Chapter 3 covers the wear of structural steel sample coupons in a slurry loop. The slurry loop is the experimental set-up that comes closest to real slurry transport. By polishing the sample until mirror-like so that the surface roughness is negligible prior to the experiments, the surface roughness after experiments is an indicator of the wear of the sample, since the roughness can solely be attributed to the wear of the sample surface. The results show that the roughness across the worn sample is, in some cases, highly non-uniform. The coupon misalignment is responsible for the non-uniform roughness profile, and the roughness profile, in turn, implies a non-uniform

wear. Since the roughness profile implies a non-uniform wear, the measurement of the wear values will be highly sample location dependent and are therefore not representative of the slurry loop conditions. These findings do not directly evaluate the comparison between fresh water and sea water, but suggest that sample size, flush mounting and wear measurement are critical to study wear in slurry loop, and roughness as an indicator of wear is highly useful. From the measurements no indication can be obtained that wear in sea water is more severe than wear in fresh water.

In chapter 4, a new finding of interaction mechanism between corrosion and abrasive wear is presented for a structural steel. Distinctively different from the enhanced effect of corrosion on wear like presented in chapter 3 due to the cyclic formation and removal of corrosion products, corrosion is able to reduce wear because of the micro-coupling effect occurring between phases with different electrochemical potentials, leading to a modified surface with enhanced abrasive wear resistance. In the study presented in chapter 4, using a structural steel as samples, the micro-coupling effect occurs between two phases: ferrite and cementite. Ferrite is electrochemically more active relative to cementite in the coupling, and therefore it is dissolved first in the corrosive environment, leading to the protruding of cementite. The protruded cementite is subsequently redistributed by abrasion, resulting in a surface layer enriched in cementite. Since cementite is much harder than ferrite, the sample surface becomes more wear resistant. Cathodic protection experiments verified the influence of corrosion. The increased wear rate under cathodic protection confirms the fact that corrosion can increase the wear resistance by modifying the surface of the sample. These findings have to be taken into account when selecting materials for use in abrasive corrosive environments.

In slurry transport field, the beneficial effect of corrosion is not observed and reported. The experience is that in sea water, the materials wear at least comparable with in fresh water, or wear faster. Therefore, the surface

modification mechanism, presented in chapter 4, cannot be the dominant process in real slurry transport. In chapter 5, the effect of impacting on the steel sample is studied. It is shown that when the impacting effect is small, corrosion still plays a dominant role so that the wear mechanism is dominated by electrochemically induced surface modification, which leads to lower wear rate in the corrosive environments than in the non-corrosive environments. As in the study presented in chapter 4, the sample in sea water wears the least compared to the cases in deionized water or ethanol. However, when the impacting effect becomes larger, the wear rates of three liquids do not show a noticeable difference, because the wear mechanism changes from abrasive material removal to chipping and plastic deformation. The influence of corrosion in the high impacting regime becomes less important and negligible. These findings show the importance to distinguish between abrasive- and impacting-wear in corrosive and non-corrosive environments.

Samenvatting

In de baggerindustrie worden jaarlijks grote hoeveelheden modder verpompt. De pijpen die hiervoor gebruikt worden, zijn sterk aan slijtage onderhevig. Dit proefschrift beschrijft de materiaalkundige aspecten hiervan.

Inzicht in het slijtgedrag is essentieel voor de juiste materiaalkeuze voor pijpen, in het bijzonder betreffende de levensduur en kosten. Slijtvastheid is geen intrinsieke materiaaleigenschap, maar eerder een systeemeigenschap, gekarakteriseerd door de combinatie van materialen die in contact zijn, hun fysieke belastingscondities en de omgevingscondities waarbinnen het contact plaatsvindt. In het geval van pijpleidingen in de baggerindustrie gaat slijtage gepaard met corrosie. Slijtage en corrosie kunnen elkaar versterken waardoor materiaal sneller kan bezwijken. In dit onderzoek wordt aandacht besteed aan de interactie tussen slijtage en corrosie, met als doel het materiaalselectieproces verder te verbeteren. Het slijtagegedrag is in kaart gebracht met een pin-on-disc tribometer, waarmee de belasting, de relatieve snelheid en de omgevingscondities van het contact voorgeschreven kunnen worden. Daarnaast kunnen de elektrochemische condities voor het pin-disc contact worden geregeld met een potentiostaat circuit.

Hoodstuk 1 beschrijft de context van het probleem en identificeert de uitdagingen die overwonnen dienen te worden. Slijtage en corrosie worden beschreven, gevolgd door een samenvatting van onderzoek in dit vakgebied. Vervolgens worden de methodes om de interactie tussen slijtage en corrosie te onderzoeken kort belicht.

Hoofdstuk 2 laat zien dat het herhaaldelijk aangroeien en wegslijten van

corrosie producten het slijtagemechanisme is van 7075-T6 aluminium in een corrosieve abrassieve omgeving. Vergelijkende experimenten laten zien dat de slijtage sterker is in een omgeving van zeewater dan in een omgeving van gedeïoniseerd water en alcohol. De slijtage met een anodische potentiaal is sterker dan de slijtage zonder potentiaal of met een kathodische potentiaal. Bovendien neemt de slijtage toe met een toenemende anodische potentiaal. Hiermee wordt aangetoond dat corrosie slijtage versterkt. De slijtage in alcohol is meer dan 20 maal minder dan in zeewater. Indien een cathodische potentiaal wordt opgelegd, dan treedt normaal gesproken cathodische bescherming op. De slijtage van de experimenten met alcohol als omgevingsvloeistof lieten echter geen verminderede slijtage zien ten gevolge van het aanbrengen van een cathodische potentiaal. De reden hiervoor is dat cathodische bescherming enkel in staat is uniforme corrosie te onderdrukken, maar niet beschermt tegen integranulaire corrosie veroorzaakt door de versterking van precipitatie deeltjes of locale corrosie door intermetallische verbindingen.

Hoofdstuk 3 beschouwt het slijtgedrag van staal in een modderachtige omgeving. De testcondities zijn soortgelijk aan de condities waaraan pijpen in de baggerindustrie zijn blootgesteld. In deze experimenten worden gepolijste, spiegelgladde stalen proefstukken getest. De oppervlakteruwheid na de test fungeert als slijtage-indicator, aangezien de ruwheid voortkomt uit slijtage. De ruwheid na het testen is in sommige gevallen sterk homogeen. Echter, uitlijnfouten van het proefstuk resulteren soms in niet-uniforme slijtage. Aangezien de oppervlakteruwheid in deze gevallen sterk locatie-afhankelijk is, is de maat van slijtage lastig vast te stellen. Deze bevindingen dragen niet direct bij aan een vergelijking van slijtage in zoetwater of zeewater, maar laten zien dat de afmetingen van het proefstuk en de uitlijning hiervan kritisch zijn, alsmede de manier waarop de resulterende ruwheid gemeten wordt.

Hoofdstuk 4 beschrijft een nieuwe kijk op de wisselwerking tussen corrosie

en abbrasieve slijtage aan de hand van slijtageproeven met constructiestaal. In hoodstuk 3 kon de versterkende werking van slijtage en corrosie met name verklaard worden door het herhaaldelijke aangroei en afvoer van corrosieproducten. In de experimenten in hoofdstuk 4 wordt juist de beschermende werking van corrosie beschreven. Het micro-koppelingseffect tussen materiaalfasen met een verschillende elektrochemische potentiaal kan leiden tot slijtvastheid verhogende oppervlakteveranderingen. In de experimenten in hoofdstuk 4 vindt dit effect plaats tussen ferriet en cementiet. Ferriet is electrochemisch actiever dan cementiet waardoor deze fase eerder oplost in de corrosieve omgeving. Het gevolg is dat het resterende cementiet lokaal als pieken aan de oppervlakte komt. Het uitstekende cementiet wordt vervolgens door abrassieve werking over de oppervlakte verdeeld waardoor zich een harde en slijtvaste laag vormt. Experimenten met cathodische bescherming valideerden de invloed van corrosie: de toename van slijtage met cathodische bescherming laat zien dat corrosie de slijtvastheid kan verhogen door de oppervlakte-eigenschappen aan te passen. Deze inzichten zijn bruikbaar in de toepassing van materialen in abrassieve corosieve omgevingen.

In de baggerindustrie is het positieve effect van corrosie op het verminderen van slijtage tot op heden nog niet waargenomen en geraporteerd. De praktijkervaring is dat materiaal in zeewater minimaal net zo snel slijt als in zoetwater. Vandaar dat de oppervlakteaanpassingen zoals beschreven in hoofdstuk 4 in de praktijk geen dominante rol kunnen spelen. In hoofdstuk 5 wordt het effect van de impactbelasting van korrels bestudeerd. Zo lang de impactbelasting laag is, speelt corosie een dominante rol: electrochemisch geïnduceerde oppervlakteaanpassingen leiden tot een hogere slijtvastheid in corrosieve omgevingen dan in niet-corrosieve omgevingen. Net als in hoofstuk 3, is de slijtage van het proefstuk in gedeioniseerd water of alcohol lager dan in zeewater. Maar wanneer de impactbelasting van de korrels groter wordt, zijn er geen verschillende meer in slijtage tussen de

verschillende omgevingen. Dit komt omdat het slijtagemechanisme in dit geval met name bestaat uit chipping. Daardoor is de invloed van corrosie onder hoge impactbelastingen van korrels te verwaarlozen. Hiermee wordt aangetoond dat de rol van corrosie met name afhangt van de intensiteit van de impactbelasting door korrels.

Curriculum Vitæ

Yueting LIU

06-11-1985 Born in Pingdingshan, China.

Education

2013–2017 PhD candidate in Precision and Microsystems Engineering
Delft University of Technology
Delft, The Netherlands

2010–2013 MSc in Materials Science and Engineering
University of Science and Technology Beijing
Beijing, China

2005–2009 BSc in Materials Processing and Controlling Engineering
Zhengzhou University
Zhengzhou, China

List of Publications

Journal articles

4. **Yueting Liu**, G.C.A.M. Janssen, *Impacting wear of structural steel with a yield strength of 235 MPa in various liquids*. Submitted to Coatings.
3. E. A. Chemmalasseri*, **Yueting Liu***, A.M. Talmon, G. Palasantzas, G.C.A.M. Janssen, C. van Rhee, *Roughness as an indicator of wear in slurry loop experiments*. Submitted to Materials. (* These authors contributed equally to this paper)
2. **Yueting Liu**, J.M.C. Mol, G.C.A.M. Janssen, *Combined corrosion and wear of aluminium alloy 7075-T6*, Journal of Bio- and Tribo-Corrosion, **2**, 9 (2016).
1. **Yueting Liu**, J.M.C. Mol, G.C.A.M. Janssen, *Corrosion reduces wet abrasive wear of structural steel*, Scripta Materialia **107**, 92 (2015).

Other collaborative work:

1. Guangming Chen, **Yueting Liu**, Dingena Schott, Gabriel Lodewijks, *Determination of the Coefficient of Sliding Wear Under Iron Ore Handling Conditions*. Submitted to Tribology Transactions.

Oral presentations:

3. **Yueting Liu**, G.C.A.M. Janssen, *Materials Innovation Institute annual conference*, Nieuwegein, The Netherlands, 12-13 December, 2016
2. **Yueting Liu**, G.C.A.M. Janssen, *Materials Science and Engineering Conference*, Darmstadt, Germany, 27-29 September, 2016
1. **Yueting Liu**, G.C.A.M. Janssen, *Euro Friction, Wear and Wear Protection Conference*, Karlsruhe, Germany, 6-8 May , 2014

Acknowledgements

Around four years ago, I started my PhD in Delft. This long journey is now approaching the end, full of wonders, frustrations, and surprises. In retrospect, I know I own thanks to many people who made my PhD experience so memorable.

First and foremost, I would like to express my profound gratitude to my supervisor, also my promotor, prof. Guido Janssen, without whom, I would not have been here. In academic aspect, I am a person who can easily drop down a rabbit hole, struggling, not knowing when to stop. Guido gave me enormous guidance and helped me decide when to start writing and when to start reviewing. The influences of these lessons are beyond academic activities, helping me become a better man. In addition to academic guidance, I appreciate the sense of humor which spiced up my PhD journey.

In addition to my supervisor, I would like to thank dr. Arjan Mol for playing an important role in my PhD, especially in performing electrochemical experiments and interpreting the data. I would like to thank Materials Innovation Institute (m2i) for sponsoring my PhD, along with three industrial partners: Boskalis, IHC, and Van Oord. I would like to show special thanks to Irina Bruckner, Marjolein Blankenstein, Gitty Bouman, Monica Reulink, Bert van Haastrecht, and other m2i colleagues for helping me get started in Holland.

My life in Delft was enjoyable with the help of a lot of people. The most support I got was from MNE group, including Alkisti, Alexandre, Andre, Cristina, Eda, Eleonoor, Enrique, Federico, Girish, Hugo, Jaap, Kai Wu, Paola, Shouen Zhu, Tjitte-Jelte, Wojciech, Yujian Huang, Murali, Ivan, Marcel, Urs, Luigi,

and Farbod. Additionally, I would like to thank my office mates and coffee buddies: Banafsheh, Selman, Sanne, Jian Zhang, Emiel, Rob Dedden, Qi Wang, Yabin Yang, Yong Zhang, Yi Zhang, Deepak, Ruijun Deng, Rajit, Max, Sasan, Evert, Gijs, Laura, and Roy. Special thanks to Rob Eling for translating my thesis summary into Dutch and also for his countless help in the past years. Thank the supporting members: Gaby, Corinne, Birgit, Marli, Marianne, Eveline, and Lisette for their solid support. I got a lot of support from our amazing technicians: Rob Luttjeboer, Patrick, Harry, and Jos. Also I used a lot of help from MSE colleagues including Sander van Asperen, Agnieszka, Maria, Zhi Sun, Ruud, Marcel Sluiter, and Kees Kwakernaak.

Many unforgettable memories are from my close Chinese friends. Especially Daijie He, Sixin Chen, Fei Yan, Anqi Fu, Yu Xin, Yexian Wu, and Chuang Yu, we travelled together, played pokers together, and cooked together. I would also like to thank Qujiang Lei, Yongwei Wang, Lian Liu, Mingjuan Zhao, Liang Xu, Xiaoqin Ou, Jun Wu, Yageng Li, Guangming Chen, Xiangyu Zhang for the friendships during the past years.

Separately, I would like to say a few words to Jie Zhou, Yixiao Wang, Peiyao Luo, and Long Wu. Jie, I got influenced by your strong sense of responsibility and that has become part of me. Long, Yixiao, and Peiyao, we have been living together for over two years as of writing this acknowledgements. You are my family in Holland. Yixiao, you are like a younger sister to me. Through ups and downs, we always support and care each other; Peiyao, you master of the art of listening and are always there when I want to share my feelings; Long, you have a beautiful heart and a creative mind, to which I attribute lots of my fun moments. It hurts to leave anyone of you. I value everyday of my life because of you.

I am grateful to the rise of China and the openness of Holland. When my parents were young, they were worried about getting enough food. They never even thought about leaving the hometown, let alone going abroad to do a PhD. Now my concern is sometimes about which journal to submit my

paper, or sometimes which country to travel to. Without a rising China, I would have been living a totally different life. In addition to my motherland, I am extremely grateful to the amazing Holland. I have met so many amazing Dutch people, polite, open-minded, kind-hearted, tall not only in appearance, also deep inside. Holland will always be my second home.

Finally it is time to thank my parents. I was raised in a culture, where people do not explicitly express emotional bond. But at the moment, I just want to say, Papa and Mama, I love you! I love you both so much that I cannot hold my tears while typing these words. I shall never forget the simple yet powerful lesson you taught me: be good and be nice. I will fight to become the best version of myself to make you feel proud. 爸爸妈妈，还有姐姐，不知何以表达这么多年你们对我的爱和支持。三十而立，依然在外漂泊，每每想到你们，我都会不能自已。你们教会我做人要善，对人要谦恭礼让，从不敢忘记。我会一直奋斗，只为看到你们脸上的笑容和骄傲！

Yueting Liu
September 2017 in Delft